AD-780 277

SPUTTERED THIN FILM RESEARCH

Alexander J. Shuskus, et al

United Aircraft Laboratories

Prepared for:

Office of Naval Research
Advanced Research Projects Agency

May 1974

Unclassified

SECURITY CLASSIFICATION OF THIS PAGE (When Data Entered)

REPORT DOCUMENTATION PAGE		READ INSTRUCTIONS BEFORE COMPLETING FORM
1. REPORT NUMBER N921337-12	2. GOVT ACCESSION NO.	3. RECIPIENT'S CATALOG NUMBER AD-780277
4. TITLE (and Subtitle) Sputtered Thin Film Research		5. TYPE OF REPORT & PERIOD COVERED Semi-Annual Report for the period 1 October 1973 to 30 April 1974
		6. PERFORMING ORG. REPORT NUMBER
7. AUTHOR(s) A. J. Shuskus, D. J. Quinn, E. L. Paradis, J. M. Berak, and D. E. Cullen		8. CONTRACT OR GRANT NUMBER(s) N00014-72-C-0415
9. PERFORMING ORGANIZATION NAME AND ADDRESS United Aircraft Research Laboratories East Hartford, Connecticut 06108		10. PROGRAM ELEMENT, PROJECT, TASK AREA & WORK UNIT NUMBERS ARPA order #2173
11. CONTROLLING OFFICE NAME AND ADDRESS Advanced Research Projects Agency 1400 Wilson Boulevard Arlington, Virginia 22209		12. REPORT DATE May 1974 13. NUMBER OF PAGES
14. MONITORING AGENCY NAME & ADDRESS (if different from Controlling Office) Department of the Navy Office of Naval Research 800 North Quincy Street Arlington, Virginia 22217		15. SECURITY CLASS. (of this report) Unclassified 15a. DECLASSIFICATION/DOWNGRADING SCHEDULE

16. DISTRIBUTION STATEMENT (of this Report)

17. DISTRIBUTION STATEMENT (of the abstract entered in Block 20, if different from Report)

18. SUPPLEMENTARY NOTES

19. KEY WORDS (Continue on reverse side if necessary and identify by block number)

Thin films, reactive sputtering, single crystal, zinc oxide, neodymium ultraphosphate, optical waveguiding, gallium nitride, tungsten oxide, epitaxy

20. ABSTRACT (Continue on reverse side if necessary and identify by block number)

Amourphous films of neodymium ultraphosphate and neodymium lanthanum ultraphosphate have been deposited by r.f. sputtering. Optical waveguide structures were fabricated and scattering losses were measured to be less than 1dB/cm. Fluoresence lifetime measurements of Nd^{3+} are presented. Data on growth of single crystal films of gallium nitride and tungsten trioxide by reactive sputtering is given. Reduced scattering losses in optical waveguide structures of zinc oxide grown on sapphire have been effected by reduction of secondary

DD FORM 1 JAN 73 1473 EDITION OF 1 NOV 65 IS OBSOLETE

I

Unclassified

SECURITY CLASSIFICATION OF THIS PAGE (When Data Entered)

20. Continued

electron bombardment of the substrate during film growth. Data is presented on the effect of magnetic field configuration on suppressing secondary electron bombardment and its effect on film uniformity.

II

UNITED AIRCRAFT CORPORATION
REASEARCH LABORATORIES
East Hartford, Connecticut

N921337-12

Fourth Semi-Annual Report Under Contract N00014-72-C-0415
1 October 1973 to 30 April 1974

ARPA Order No.:	2173, Amendment No. #2/07-26-73
Program Cost Code:	000003D10K21
Contractor:	United Aircraft Research Laboratories
Effective Date of Contract:	15 April 1972
Contract Expiration Date:	30 September 1974
Amount of Contract:	$422,005.00
Contract Number:	N00014-72-C-0415
Contract Management:	Dr. Anthony J. DeMaria (203)565-3545
Principal Investigator:	Dr. Alexander J. Shuskus (203)565-6498
Scientific Officer:	Dr. Van Nicolai
Short Title:	Sputtered Thin Film Optics
Reported By:	A. J. Shuskus, D. J. Quinn, E. L. Paradis, J. M. Berak and D. E. Cullen

Sponsored by Advanced Research Projects Agency
ARPA Order No. 2173, Amendment No. #2/07-26-73

III

Report N921337-12

Interim Technical Report Under Contract N00014-72-C-0415
for the Period 1 October 1973 through 30 April 1974

Sputtered Thin Film Research

ARPA Order No. 2173, Amendment No. 1, Project Code 3D10

TABLE OF CONTENTS

	Page
LIST OF ILLUSTRATIONS	iii
LIST OF TABLES	v
1.0 TECHNICAL REPORT SUMMARY	1-1
1.1 Program Objective	1-1
1.2 Major Accomplishments	1-1
1.3 Future Work	1-2
2.0 GROWTH OF SPUTTERED LASER MATERIALS	2-1
2.1 Growth of Ultraphosphate Bulk Crystal	2-1
2.2 Growth of Neodymium Ultraphosphate Films	2-3
2.3 Optical Characterization of the Ultraphosphates	2-5
2.4 Optical Absorption	2-5
2.5 Fluoresence Lifetime	2-6
2.6 Waveguide Attenuation in Sputtered NdUP Films	2-9
2.7 Laser Applications of Ultraphosphate Glasses	2-10
3.0 GROWTH OF EPITAXIAL GALLIUM ARSENIDE FILMS	3-1
4.0 EPITAXY OF GALLIUM NITRIDE BY REACTIVE SPUTTERING	4-1

TABLE OF CONTENTS
(cont'd)

Page

4.1 Epitaxial Thin Film Deposition. 4-1
4.2 Future Work 4-2

5.0 TUNGSTEN TRIOXIDE. 5-1

6.0 OPTIMIZATION OF ZINC OXIDE DEPOSITION PARAMETERS 6-1

6.1 Magnetic Field Experiments. 6-1
6.2 Substrate Heater Temperature Experiments. 6-3
6.3 Target Power Input Experiments. 6-4
6.4 Gas Pressure Experiments. 6-4

7.0 REFERENCES 7-1

LIST OF ILLUSTRATIONS

Figure 2.1 RED of Neodymium Ultraphosphate (#6)

Figure 2.2 Absorption Spectra of Sputtered and Bulk Neodymium Ultraphosphate

Figure 2.3 Experimental Set Up Used for Fluoresence Lifetime Measurements

Figure 2.4 Infrared Fluoresence Decay Curves for Bulk Ultraphosphates

Figure 2.5 Infrared Fluoresence Decay Curve for Sputtered Thin Film Neodymium Ultraphosphate (#14)

Figure 2.6 Infrared Fluoresence Decay Curve for Sputtered Neodymium-Lanthanum Ultraphosphate Glass

Figure 2.7 Fluoresence Lifetime Determination for NdUP#14 and NdLaUP#15 Sputtered Films

Figure 2.8 Schematic of Waveguide Assembly

Figure 2.9 Schematic of Thin Film Laser Cavity

Figure 2.10 Thin Film Laser Cavity

Figure 4.1 RED of GaN on (0001) Sapphire

Figure 4.2 RED of GaN on $(1\bar{1}02)$ Sapphire

Figure 5.1 RED of WO_3 on $(1\bar{1}02)$ Sapphire

Figure 6.1 Schematic of the Major Internal Components of the Sputtering System

Figure 6.2 Sensor Temperature Rise as a Function of Time After Start Up Recorded for a Quadrupole Magnetic Field Configuration

Figure 6.3 Comparison of Deposition Rate and Substrate Temperature Profiles for Several Quadrupole Field Configurations

Figure 6.4 Comparison of Deposition Rate and Substrate Temperature Profile for a Longitudinal Field Configuration

Figure 6.5 Electron Micrograph of ZnO Film Sputtered on $(1\bar{1}02)$ Oriented Sapphire Substrate

Figure 6.6 Scattering Loss of ZnO Film

LIST OF TABLES

Table 2-1 Summary of Growth Conditions for Bulk NdP_5O_{14}

Table 2-2 Determination of Film Stoichiometry by Electron Microprobe Analysis

Table 2-3 Summary of Flouresence Lifetime for Ultraphosphate Samples

1.0 SUMMARY

1.1 Program Objective

The major objective of the program is to extablish the feasibility of reactive rf sputtering for the preparation of single crystal thin films suitable for elctronic and integrated optics applications. Materials of interest include selected III-V and II-VI semiconductors, high dielectric constant materials and neodymium ultraphosphate. A secondary objective of the program is the fabrication of devices to ascertain the device potential of the material prepared by reative sputtering. This research program is being conducted under the ARPA/ONR Contract No. N00014-72-C-0415.

1.2 Major Accomplishments

Bulk material of neodymium ultraphosphate (NdP_5O_{14}) and neodymium lanthanum ultraphosphate ($Nd_{0.5}La_{0.5}P_5O_{14}$) was synthesized to provide target material for sputtering of ultraphosphate films. Amorphous films of the ultraphosphate were deposited on 7059 glass substrates by rf sputtering in an oxygen ambient. The films exhibited low optical loss, less than 1dB/cm. These results are encouraging because low loss films are required if a thin film laser is to be fabricated with this material. The neodymium fluoresence lifetime at 1.052μ in the NdP_5O_{14} glass was observed to be 8 μsec and 16 μsec in the $Nd_{0.5}La_{0.5}P_5O_{14}$ glass. A special fixture has been designed and fabricated to evaluate the films for laser action.

Single crystal films of gallium nitride have been successfully grown on (111) oriented substrates of magnesium aluminum spinel and (0001) and (1102) oriented sapphire substrates. The films are clear and insulating. To our knowledge this work constitutes the first successful report of the growth of epitaxial gallium nitride films by reactive sputtering.

Through modifications to the sputtering system, primarily by appropriate tailoring of the magnetic fields. secondary electron bombardment of the substrate has been reduced considerably. This has resulted in the growth of much improved zinc oxide films. Optical loss at 6328 Å has been reduced from 18dB/cm to 5dB/cm. Optical loss at 1.06μ has been reduced to less than 1dB/cm. Acoustooptic and electrooptic modulators have been constructed and are currently undergoing evaluation.

Epitaxial growth of tungsten trioxide has been obtained on (110) spinel and $(1\bar{1}02)$ sapphire substrates. The tungsten trioxide grows with (010) planes paralled to the surface. The films are twinned as a result of domain formation

and this results in excessive loss in optical waveguide structures. Unless epitaxy can be achieved at lower temperatures the twinning precludes the use of tungsten trioxide in optical waveguide structures.

1.3 Future Work

The optical characterisitics of the ultraphosphate films will continue to be evaluated. If laser action is observed in films with the use of external mirrors, distributed feedback laser structures will be fabricated for evaluation.

Piezoelectric properties of the gallium nitride films will be evaluated by the fabrication of surface acoustic wave delay lines. Optical attenuation losses in waveguide structures will be made. Doping of the insulating gallium nitride films formed by reactive sputtering will be explored.

With preparation of low loss optical waveguides with sputtered zinc oxide, acoustoopic modulators will be fabricated for further evaluation of the material.

2.0 GROWTH OF SPUTTERED LASER MATERIALS

Considerable progress has been achieved in growing films of neodymium-containing phosphate glass by using rf sputtering and will be described in this section of the report. Optically, the films exhibit low loss at the laser frequency and possess an encouragingly high fluorescence lifetime. In addition, the growth of bulk ultraphosphate crystals of composition NdP_5O_{14}, $Nd_{0.5}La_{0.5}P_5O_{14}$, and $Nd_{0.99}Dy_{0.01}P_5O_{14}$ is discussed. Bulk crystals are required in order to (1) provide target material and/or (2) establish a reference value of the fluorescence lifetime to which measured values of the film can be compared.

2.1 Growth of Ultraphosphate Bulk Crystals

The rare-earth 4f ultraphosphates were prepared by heating the transition metal oxide (99.9% to 99.99% pure) with phosphoric acid (electronic grade) to about 500°C to 700°C in an Au or PdAu crucible under a dry oxygen flow. In the process, water is preferentially lost to form higher phosphoric acids, and a transition metal ultraphosphate, MP_5O_{14}, is eventually crystallized out of solution. As a part of the heating schedule (before raising the crucible to high temperatures) the reactants are held at ∿ 250°C to 300°C to ensure dissolution of the oxide. Table 2-1 summarizes the growth conditions for the MP_5O_{14} runs. In all cases the amount of phosphoric acid initially present is greater than that required to form the ultraphosphate. In order to form only the composition MP_5O_{14}, the ratio (moles H_3PO_4)/(moles M_2O_3) must be equal to 10. The numbers in the third column, then, are an indication of the excess phosphoric acid initially present in the crucible. In the more dilute solutions the crystals tended to be larger and more perfect (as expected) whereas smaller crystallites were produced in the more concentrated solutions. Growth out of concentrated solution was necessary in order to synthesize sufficient material to fabricate a target in a minimum number of growth runs. A minimum of fifty grams of ultraphosphate was necessary to cover a 4-inch diameter target, whereas ∿ 150 grams was necessary for a pressed target. The growth runs were terminated when no visible vapors from further decomposition of the polyphosphoric acid could be seen coming out of the crucible. After removal from the crucible, the ultraphosphates were digested in hot water to remove any unreacted species of phosphoric acid. Lifetime measurements, which will be described in Section 2.5 and compared to the literature values, are listed in the last column of Table 2-1. The growth conditions summarized in this table did not significantly affect the measured lifetimes for either NdP_5O_{14} or $Nd_{0.5}La_{0.5}P_5O_{14}$.

TABLE 2-1

Summary of Growth Conditions for Bulk MP_5O_{14}

* Run No.	** Reagents	Moles H_3PO_4 / Moles M_2O_3	Composition	Temp (°C)	Time (hrs)	Lifetime τ (μsec)
2M	Nd_2O_3-MC	11.8	NdP_5O_{14}	500	20	100
3M	Nd_2O_3-MC	10.9	NdP_5O_{14}	500	20	
4M	Nd_2O_3-MC	10.9	NdP_5O_{14}	500	20	
5M	Nd_2O_3-MC	11.0	NdP_5O_{14}	475	20	
6M	Nd_2O_3-MC	130	NdP_5O_{14}	550	140	96-120
7M	Nd_2O_3-MC La_2O_3-BR	127	$Nd_{0.50}La_{0.50}P_5O_{14}$	550	140	160
8M	Nd_2O_3-MC Dy_2O_3-BR	135	$Nd_{0.99}Dy_{0.01}P_5O_{14}$	600 +(725)	70 +(∿1)	22
9M	Nd_2O_3-MC	22	NdP_5O_{14}	575	190	--
10M	Nd_2O_3-MC La_2O_3-BR	19	$Nd_{0.50}La_{0.50}P_5O_{14}$	625	96	190
11M	Nd_2O_3-MC La_2O_3-BR	28	$Nd_{0.50}La_{0.50}P_5O_{14}$	625	96	--
12M	Nd_2O_3-M La_2O_3-M	30	$Nd_{0.50}La_{0.50}P_5O_{14}$	575	190	200

* Runs 2M to 5M - use Pd-Au crucible
Runs 6M to 12M - use Au crucible

** All runs employ electronic grade phosphoric acid
Reagent Code: MC - Michigan Chemical Corporation - 99.9% pure
BR - Bernard Ring - 99.9% pure
M - Molybdenum Corp. of America - 99.99% pure

2.2 Growth of Neodymium Ultraphosphate Films

Amorphous films containing neodymium, phosphorous, and oxygen and having low optical loss (< 1 dB/cm) have been fabricated using rf sputtering of a NdP_5O_{14} target. During sputtering, both polycrystalline and/or amorphous films can be grown. Since polycrystalline films of this material are useless for waveguide application due to the extremely high scattering caused by the crystallites, studies are underway to characterize the deposition parameters for formation of the amorphous phase. It can be said at this point, however, that the amorphous phase can only be grown over a narrow temperature range. At higher temperatures, polycrystalline films are formed while at lower temperatures decomposition products condense as a viscous liquid on the substrate. It has also been ascertained that a partial pressure of oxygen is required during sputtering to prevent the formation of brown oxygen-deficient films. These factors will be discussed in detail in the next report when our knowledge of the boundary conditions for amorphous growth will be known with a greater degree of certainty. Fig. 2-1 shows RED patterns of a sample deposited near the upper transition temperature and had both cloudy and transparent areas which were sputtered during one growth run onto 7059 glass - this is the substrate material used for all the ultraphosphate depositions. The diffuse halos of the amorphous (transparent) area are to be compared with the additional ring patterns generated by the clouded polycrystalline area.

Although the sputtered films will be referred to in this report as ultraphosphate films, the analyzed phosphorous-to-neodymium atomic ratios are less than the value 5 as in the ultraphosphate. This is illustrated by the electron microprobe results in Table 2-2 for various Nd ultraphosphate films. For purposes of this analysis, a single crystal of NdP_5O_{14} selected from growth run #6M was used a reference. Counts were taken in an alternate fashion between the standard and each of the three sputtered films, and this was repeated ten times for each element (neodymium and phosphorous). Oxygen was determined by difference, since the neodymium line interferes with the K-α oxygen line. In addition, general analyses showed the absence of other atomic constituents (to within five-tenths of a percent). The particular results show that the NdUP films are neodymium rich and phosphorous deficient and the atom ratio, P/Nd, varies between 2.8 and 3.3. That the P/Nd ratio is low is expected on the basis of the greater volatility and the generally lower sticking coefficients of phosphorous compounds compared to neodymium. This suggests that the amorphous films should be sputtered at as low a temperature as possible consistent with formation of the solid amorphous phase. This would have the added advantage of reducing interfacial stresses which may develop between the sputtered film and substrate as the sample is cooled to room temperature after growth. An alternative route to raising the phosphorous content in the film would be to add phosphorous or phosphorous pentoxide to the NdP_5O_{14} target. This would raise the partial pressure of phosphorous containing species in the plasma and ultimately in the

TABLE 2–2

DETERMINATION OF FILM STOICHIOMETRY BY ELECTRON MICROPROBE ANALYSIS

MEAN CHEMICAL COMPOSITIONS AND TWO SIGMA LIMITS BASED ON TEN ANALYSES

ATOMIC PERCENT

	STANDARD	NdUP # 2	NdUP # 7	NdUP # 14
Nd	5	6.69 ± 0.17	7.14 ± 0.37	6.36 ± 0.54
P	25	22.35 ± 0.48	19.56 ± 1.74	18.41 ± 1.32
O	70	70.96 ± 0.64*	73.30 ± 2.08*	75.23 ± 1.76*

ATOMIC PERCENT

	STANDARD	NdLa UP # 15
Nd	2.5	4.89 ± 0.11
La	2.5	4.95 ± 0.12
P	25	22.10 ± 0.68
O	70	68.06 ± 0.77*

* DETERMINED BY DIFFERENCE

deposited film. It is not clear, however, whether phosphorous deficiency will have a deleterious effect on the optical properties of the films. Other variables which may be more important in affecting laser performance are absolute neodymium concentration (self-quenching), stress, and certain impurities. It has been demonstrated in the literature (Ref. 1) and in this report that lanthanum substitution in neodymium ultraphosphate bulk material improves the fluorescence lifetime by reducing self-quenching between neodymium ions. Since the composition, $Nd_{0.5}La_{0.5}P_5O_{14}$ has been suggested as an optimum one, material was selected from growth run #10M to be used as target material for sputtering of an ultraphosphate film containing neodymium and lanthanum. The electron microprobe results are shown in Table 2-2. The phosphorous content is similar to the NdUP layers but the measured high neodymium and lanthanum concentrations cannot be explained. A consistent factor is the close agreement in the Nd and La concentrations in the film. This indicates that the sticking coefficients for these elements are nearly the same and that their relative compositions in the film can be varied by suitable adjustment of their compositions in the target.

2.3 Optical Characterization of the Ultraphospates

Important material properties for laser application are (1) low loss at the lasing wavelength due either to absorption or scattering, (2) long fluorescence lifetime, which is affected by stress, imputities, and fluorescence quenching due to cross relaxation between active ions, and (3) optimization of the active ion concentration in order to balance gain versus heat dissipation.

The subject of this section will be a discussion of the experimental techniques and results of absorption and fluorescence lifetime measurements of bulk and thin film ultraphosphate samples. An upper limit on the scattering losses in the sputtered films has also been established.

2.4 Optical Absorption

A Cary spectrometer was used to obtain the absorption spectra of the ultraphosphate samples shown in Fig. 2-2. As can be readily seen, no major absorption occurs in the region of 1.05 μm, and the neodymium pump bands are located in the same regions as the bulk. At the Ar-ion laser wavelength of 0.5145 μm, the film has an absorption coefficient of $\alpha = -22\ cm^{-1}$. This wavelength has successfully been used to pump the neodymium ion. All of the absorption measurements of bulk and film ultraphosphate materials have the same absorption spectra.

2.5 Fluorescence Lifetime

The fluorescence lifetime was determined by pumping an ultraphosphate sample with a 1.5 μsec pulse at 0.5900 μm wavelength from a Rhodamine-6G dye laser. The experimental set up is summarized in Fig. 2-3. About 100 millijoules of power pass through a KG-3 IR absorbing filter and onto either the sputtered film or a collection of bulk crystals sandwiched inside an O-ring between 2 glass slides. Both the visible laser light and that generated as photoluminescent radiation strike an optical filtering network consisting of a bandpass interference filter and two visible absorbing filters placed in front of the detector. The bandpass filter allows a peak transmission at 1.062 μm of 75%, and this falls by 50% at 165 Å on either side of this wavelength. Thus, the most intense room temperature fluorescence line at 1.051 μm (Ref. 2) will pass with minor attenuation. Additional visible cut-off filters attenuate infrared light above 0.8 μm. Behind the filter stack is an S-1 photomultiplier detector operated at room temperature. The signal is displayed on an oscilloscope which has been triggered by the laser pulse using a silicon photocell. The overall resolution limit of the detection system is ∿ 2 μsec. Figures 2-4 to 2-6 are photographs of the fluorescence decay for selected bulk and thin-film ultraphosphates. Fig. 2-7 shows plots illustrating the method used for obtaining the fluorescence lifetime from these photographs. In all cases, good exponential behavior with time is observed. A summary of all the lifetime measurements of bulk and sputtered film samples along with literature values for bulk material is shown in Table 2-3.

Fluorescence lifetime (τ) is a critical parameter for laser materials in that the population density at the lasing threshold (N_T) of the upper state is directly proportional to this quantity, that is

$$N_T = \frac{P_T \tau}{h\nu V}, \qquad \text{Eq. 2-1}$$

where P_T is the threshold pump power and V is volume of the pumped region. In addition, τ is related to the line width ($\Delta\nu$) by

$$\tau = \frac{\lambda^2}{8\pi^2 n^2 \Delta\nu \delta_o} \qquad \text{Eq. 2-2}$$

where n is the index of refraction, λ the wavelength, and δ_o the emission cross section. The linewidth of a particular transistion is controlled by perturbations of the local fields at the site of the active ion. These perturbations are caused by variations of the positions of the atoms surrounding the active ion. Factors which influence interatomic spacings are stress, temperature, and struc-

TABLE 2-3

Summary of Fluorescence Lifetime for Ultraphosphate Samples

	Fluorescence Lifetime (μsec)		
	Bulk UP		Sputtered Film
Composition	Literature Values	UARL	
NdUP	66**	96-120	8
$Nd_{0.5}La_{0.5}UP$	30-200**	160-200	16
$Nd_{0.99}Dy_{0.01}UP$	24*	22	-

* Reference 3
** Reference 1

tural imperfections. In the amorphous highly disordered state, each atom sees a slightly different environment, and each active ion, therefore, has a distinct set of split energy levels. Increasing stress, temperature, or transforming from the crystalline to the amorphous state will decrease the fluorescence lifetime. In addition, cross-relaxation processes, which are a function of the interneodymium distance, result in a decrease in the fluorescence lifetime as the neodymium concentration increases. Certain impurities that have energy levels within the lasing levels will permit fast transitions to the ground state (impurity quenching), thus also shortening the fluorescence lifetime. Other impurities just serve to dilute the active ions but do not participate in the lasing process.

The measured lifetime results illustrate the general principles mentioned in the last paragraph. The literature values show the increase in lifetime with lanthanum addition which decreases the probability for cross relaxation. That dilution is possible with lanthanum is due to the facts that lanthanum is completely miscible with neodymium (nearly the same ionic radii and causing little stress), and lanthanum has no atomic levels appearing between the $^4F_{3/2}$ and $^4I_{11/2}$ neodymium fluorescence levels. Dysprosium, on the other hand, has several levels within the fluorescence bands of the neodymium ion and impurity quenching results. It has been reported in the literature (Ref. 1 and 3) that varying growth conditions (e.g., temperature and presence of impurities) affect the resultant lifetimes. This is suggested to be the reason for the wide variation in lifetimes reported for bulk $Nd_{0.5}La_{0.5}UP$ and is probably responsible for our generally higher lifetime results for bulk NdP_5O_{14} and $Nd_{0.5}La_{0.5}P_5O_{14}$. Crystal stress may also be a factor here.

With regard to the sputtered films, a decrease in fluorescent lifetime can be attributed to any or all of the following factors: (1) disorder due to the amorphous phase, (2) self-quenching due to the increased neodymium atom concentrations compared to the bulk, and (3) intrinsic stress due to the deposition process or induced stress due to mismatch of the expansion coefficients between the film and substrate. It is impossible at this time to ascertain which of these processes is the predominant one. Even though the neodymium ion is located in an amorphous structure, which may be responsible here for the short lifetime, values as high as 700 μsec have been measured for bulk Nd^{3+} in a rubidium lime silicate glass (Ref. 4). Self-quenching seems to be operative when comparing the measured lifetimes of the NdUP and NdLaUP films because a decrease in neodymium concentration from 6.36% (NdUP #14) to 4.89% (NdLaUP #15) resulted in an increase in the lifetime by a factor of two. Another interesting comparison exists between the fluorescence lifetime of NdLaUP #15 and that inferred from a glassy NdP_5O_{14} bulk sample (5 atomic % Nd) reported in the literature to have lased at about five times higher threshold that the bulk ultraphosphate (Ref. 5). If from Eq. 2.1 the assumption is made that this difference in threshold is due to a five-fold decrease in fluorescence lifetime compared to

their bulk ultraphosphate material, then the lifetime of their amorphous material is calculated to be 13 μsec. This is very close to the value, 16 μsec, for our NdLaUP #15 sputtered amorphous film. Of particular note is the fact that the neodymium concentrations are nearly the same for these two samples. If self-quenching is a factor in the amorphous films, it is reasonable to expect at least a factor of two increase in the lifetime for the amorphous films if the neodymium concentration is halved to 2.5 atom percent - this is known to be the case for the bulk material. As discussed before, changes in the constitution of the target can be made to affect this change in the film's neodymium concentration. The third factor, stress, is evident in sputtered films greater than about seven microns in thickness. The stress manifests itself as cracks which when analyzed under an optical microscope or Talysurf are accompanied by raised areas which, in one case, NdLaUP #15, were about 200 Å high and 50 microns wide. This indicates that the film is undergoing compression but whether the stress is intrinsic to the sputtering process or caused by differences in thermal contraction between the film and substrate is not known at this point. Close examination of thick films grown on substrates having an expansion coefficient smaller than $4.5 \times 10^{-6}/^{\circ}C$ (7059 glass) will resolve this difficulty in assignment of cause.

2.6 Waveguide Attenuation in Sputtered NdUP Films

Our amorphous ultraphosphate films have optical attenuation due to scattering well below 1 dB/cm. Attenuation of 1 dB/cm caused by scattering can readily be seen as a bright streak in a thin film waveguide; however, the light scattered out of the ultraphosphate films is so small that it can barely be seen by the naked eye, indicating a scattering loss of well-below 1 dB/cm. A few surface and volume irregularities do result in occasional bright points of light but these do not constitute an appreciable loss mechanism nor do they characterize the scattering from the continuum of the film. A quantitative measurement of the losses has not been made since the methods of measuring scattering losses described in Section 2.1 of the last report are not suitable for films with losses below $\sim$ 1 dB/cm.

In order to place an upper limit on the absorption losses near the laser wavelength (1.06 μm), a waveguide with input and output prism couplers was employed and is shown schematically in Fig. 2-8. The high-index prisms were bonded to the waveguide with an organic glue (aroclor) having an index intermediate between the prism and waveguide. A Nd:YAG laser was used to produce beam A, and the intensities of this beam and all the reflected beams, as well as the coupled output beam were measured. Assuming that there is a 100% coupling efficiency at both the input and output prisms, then all of the light that cannot be accounted for can be attributed to absorption in the waveguide. Since some scattered light is lost in the prisms, it is impossible to account for all of the lost light. Therefore, this measurement only places an upper limit on the film absorption.

The above results indicate that a thin film laser should be possible using sputtered NdUP. Both scattering and absorption losses are low ($< \sim 1$ dB/cm) at the laser wavelength, the absorption in the pump band is large, and the lifetime (especially for the lanthanum alloy films) appears long enough when compared to bulk values for NdP_5O_{14} glass, which has been reported to have lased. (Ref. 5).

2.7 Laser Applications of Ultraphospate Glasses

The final objective of thin-film sputtering research into growth of the ultraphosphate materials is to produce a thin-film laser which can be pumped in the plane of the film by a light emitting diode. Although loss, lifetime, and absorption measurements on the ultraphosphate glass are encouraging, it still must be demonstrated that laser action is possible. A practical integrated optic circuit would most certainly have the active laser element operating in a waveguide mode. Therefore, it would be expedient if a waveguiding laser could be successfully fabricated in order to demonstrate the entire concept. A less stringent demonstration of laser activity is the measurement of gain in a material. With this technique no feedback is necessary and the overall gain can be less than unity. The sample is pumped and coherent light of the lasing wavelength is waveguided through the film. The intensity of the output with and without the pump light is a direct measure of the optical gain of the material. Since the glass may not lase at 1.052 (the lasing line for the bulk crystals), no coherent tunable signal source is available; therefore, gain measurements cannot be done. Since the lasing characteristics of the glass are to be experimentally determined and optimized, a wider range in pump power than is possible with a state-of-the-act LED is necessary. For this reason, an argon-ion laser will be used to excite the neodymium ion. Practical techniques for pumping the ultraphosphate film include (1) focusing the beam perpendicular to the plane of the film and (2) grating or (3) prism coupling of the pump light into a waveguide mode. Since the lasing threshold of the sputtered ultraphosphate is unknown, the choice of the pumping technique must be based on maximizing the optical power absorbed in the film. The argon-ion laser line which is most strongly absorbed by the Nd^{3+} is 0.5145 μm. A sputtered neodymium ultraphospate film (#14) has a measured absorbtion coefficient of 22 cm^{-1} at this wavelength. If this film is pumped perpendicular to the film plane, fifty percent of the light will be absorbed in 315 μm of film. Practical waveguide thicknesses lie between 1 and 10 μm making this pumping technique unfeasable. Absorption of light via waveguide pumping with a grating or prism is not limited by thickness beyond the penetration depth of the evanecent wave. Both kinds of couplers possess about the same theoretical coupling efficiency; however, the fabrication $\sim 1/4$ μm grating spacings is difficult, and theoretical efficiencies are not achieved. In view of these reasons, prism coupled pumping was chosen.

Several techniques exist for providing feedback in a thin-film laser: (1) distributed feedback using a grating and (2) coupling to an external cavity using gratings or prisms. Because of the afore-mentioned problems with gratings, prism coupling to external mirrors was the initial choice as the feedback mechanism in the waveguide laser. The single pass loss of this approach had to be determined before the decision could be considered final. The results of this measurement are shown on Fig. 2-8 under "output efficiency", where a value of 13.7% has been achieved at 1.06 μm. This single pass loss of 86% is still much less than the 99.7% loss which accompanied laser action in $^{N}d_{0.99}{}^{Y}{}_{0.01}\,P_5O_{14}$ (Ref. 6). It is the high experimental gain coefficient (up to 830 cm^{-1} in $Nd_{0.5}La_{0.5}P_5O_{14}$ (Ref. 1) which is responsible for laser performance even under conditions of high cavity loss. The gain coefficient, α, in the material is equal to the emission cross section, σ, times the population density of the excited state, N_E. From Eq. 2.1, $N_E \sim P_T \tau$. The gain in the active material is therefore proportional to exp ($\sigma P_T \tau$). In the sputtered films, τ is down about an order of magnitude compared to the crystal values. Reported threshold pump powers range between 4mw and 25mw (Refs. 7 and 8). Assuming the same σ, a pump power ranging from $\sim$ 40 mw to 250 mw would be required to reach threshold for the sputtered film. With a 10% prism coupling efficiency, a 100 mw pump capability is available using the 1-watt argon-ion laser.

The general design of the prism-coupled waveguide laser is schematically shown in Fig. 2-9 and pictured in Fig. 2-10. The pump light is imaged to a line at the base of the pump coupling prism. This image is formed by a cylindrical lens placed in the chopped beam of the argon-ion laser. A fourth output prism (not shown) is placed opposite the input coupling prism and displays the pump light on a screen when the beam is properly aligned. Cavity prisms sit at right angles to the pump beam direction and are aligned with the external mirrors. The substrate is heat sunk to a water-cooled jig using gallium.

Fluorescence has been observed in the above configuration indicating a guided pump mode; however, no laser action could be identified. The 100 mw pump power available may have been insufficient to reach threshold. Furthermore, the cavity mirror alignment is very critical, and conditions for a lasing mode may not have been established. In light of the above results, an attempt is also being made to make the ultraphosphate crystals lase in a cavity composed of two closely spaced dielectric mirrors. Pumping is achieved through one of the mirrors using a 350 mJ pulsed Rhodamine 6G laser. When bulk-crystal lasing is observed, the lasing threshold of the films will be measured in order to determine if the available cw argon-ion pumping power is sufficient to effect film lasing in the waveguide configuration shown in Fig 2-9.

RED OF SPUTTERED NEODYNIUM ULTRAPHOSPHATE (#6)

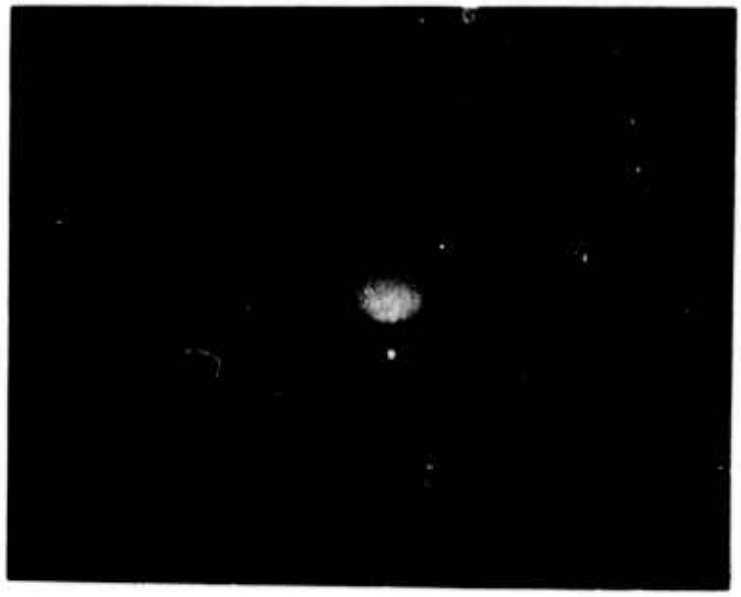

CLOUDY AREA

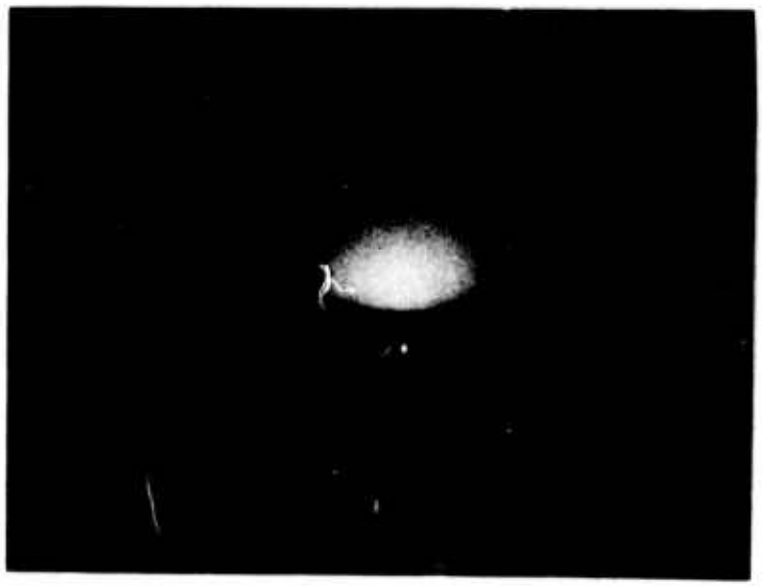

TRANSPARENT AREA

FIG. 2–2

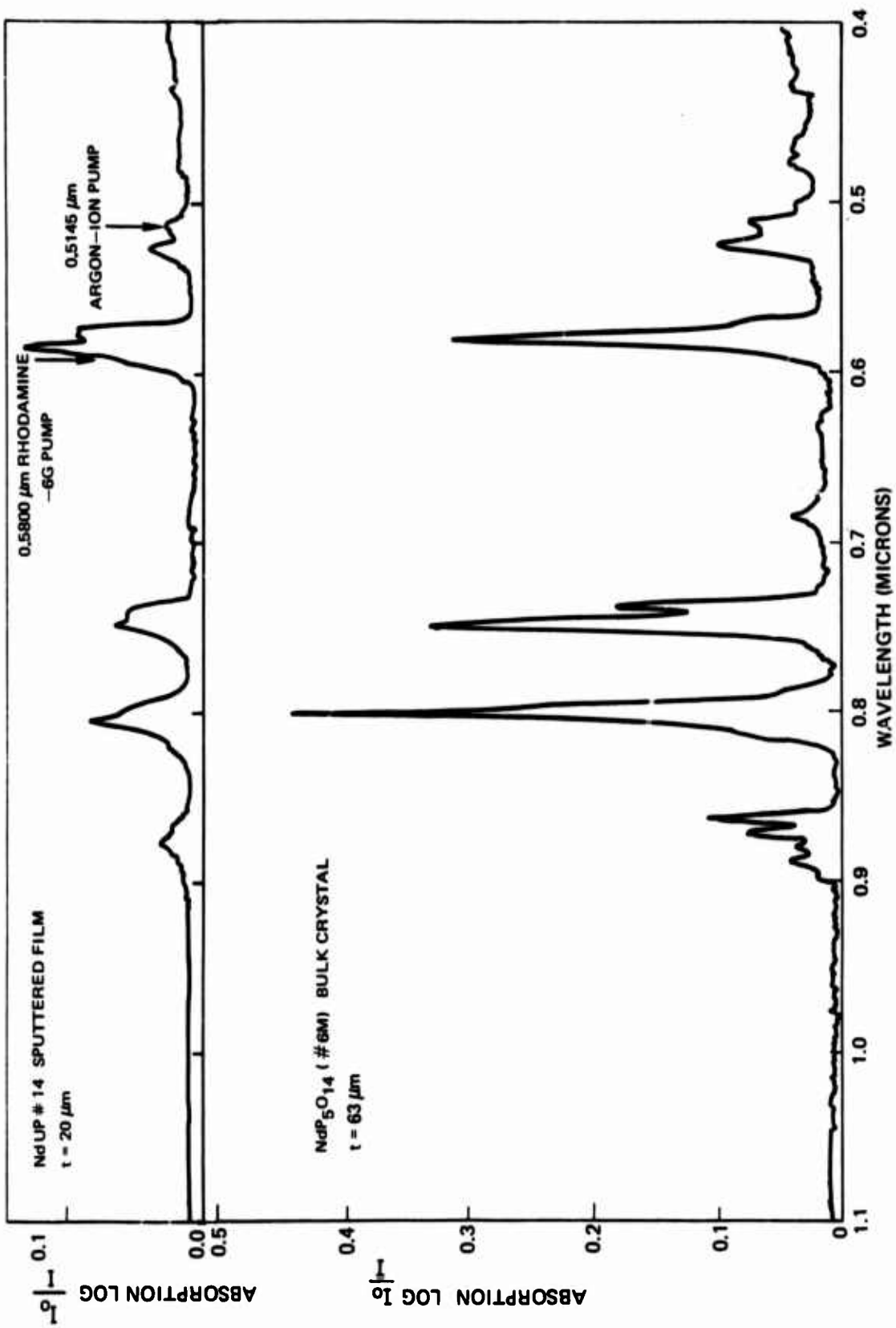

N04–198–2

FIG. 2-3

EXPERIMENTAL SET UP USED FOR FLUORESCENCE LIFETIME MEASUREMENTS

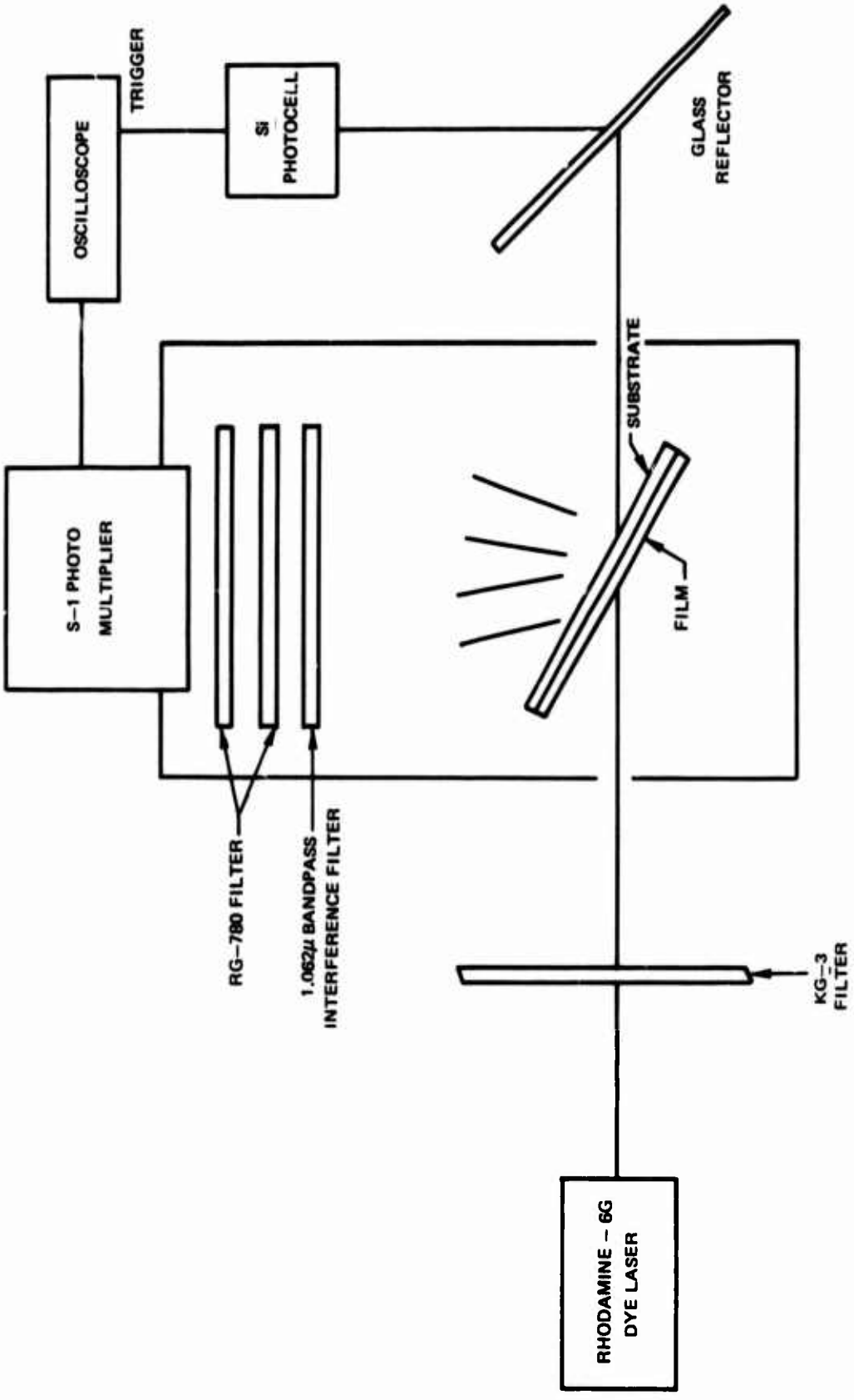

N04-181-1

INFARED FLUORESCENCE DECAY CURVES FOR BULK NEODYMIUM ULTRAPHOSPHATE (6M) AND NEODYMIUM LANTHANUM ULTRAPHOSPHATE (10M)

NdUP (τ = 96 μsec)

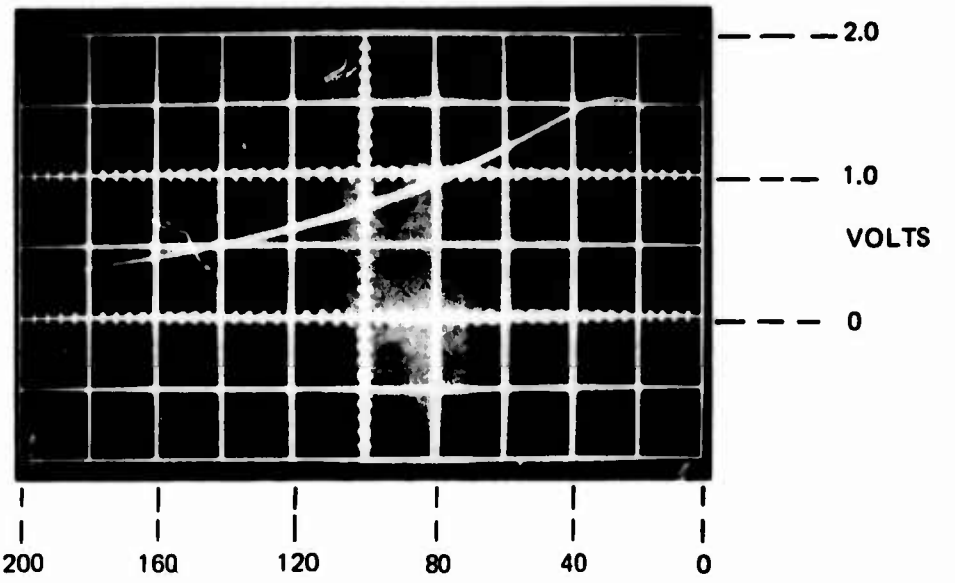

NdLaUP (τ = 190 μsec)

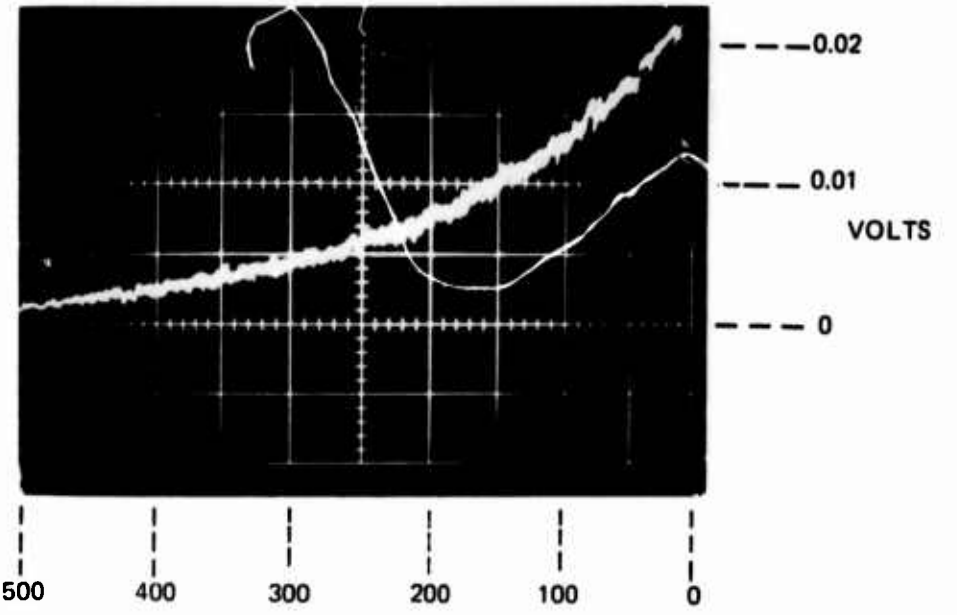

FIG. 2–5

INFRARED FLUORESCENCE DECAY CURVE FOR SPUTTERED THIN FILM NEODYMIUM ULTRAPHOSPHATE GLASS (#14)

τ = 8.3 μ sec

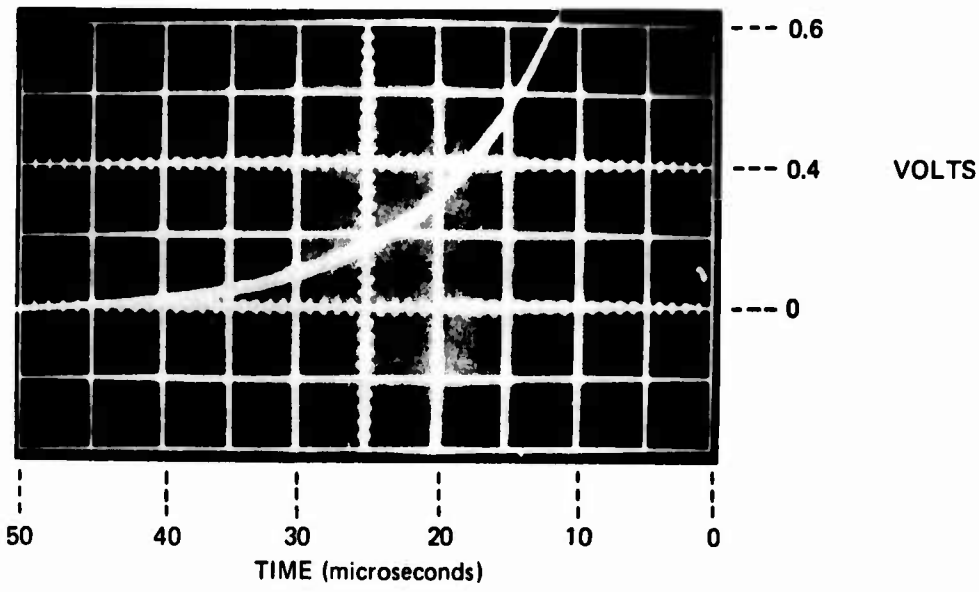

N05–15–1

INFARED FLUORESCENCE DECAY CURVE FOR SPUTTERED THIN FILM NEODYMIUM-LANTHANUM ULTRAPHOSPHATE GLASS (# 15)

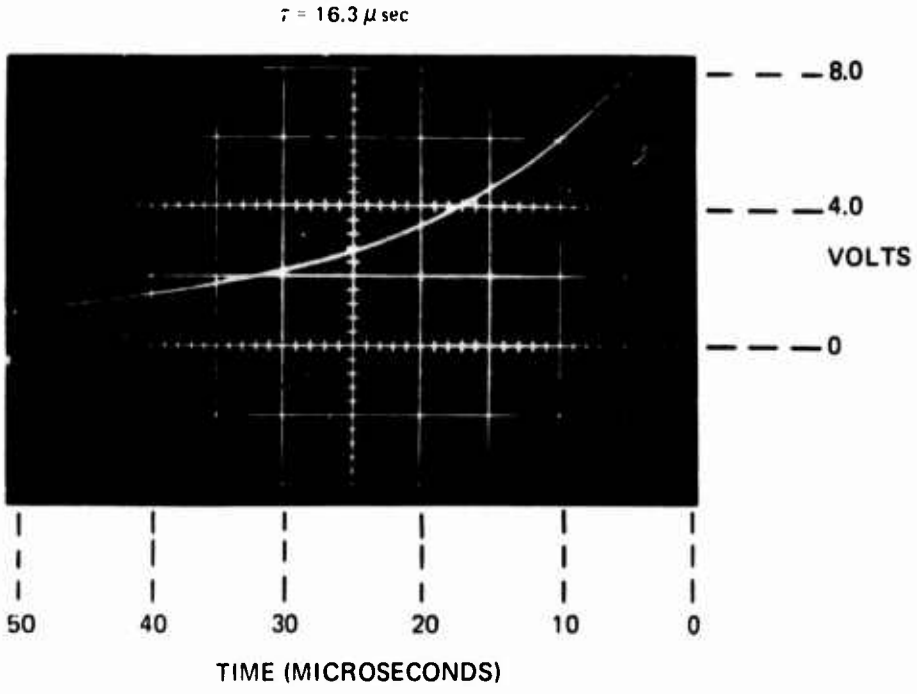

FIG. 2–7

FLUORESCENCE LIFETIME DETERMINATION FOR NdUP #14 AND NdLaUP #15 SPUTTERED FILMS

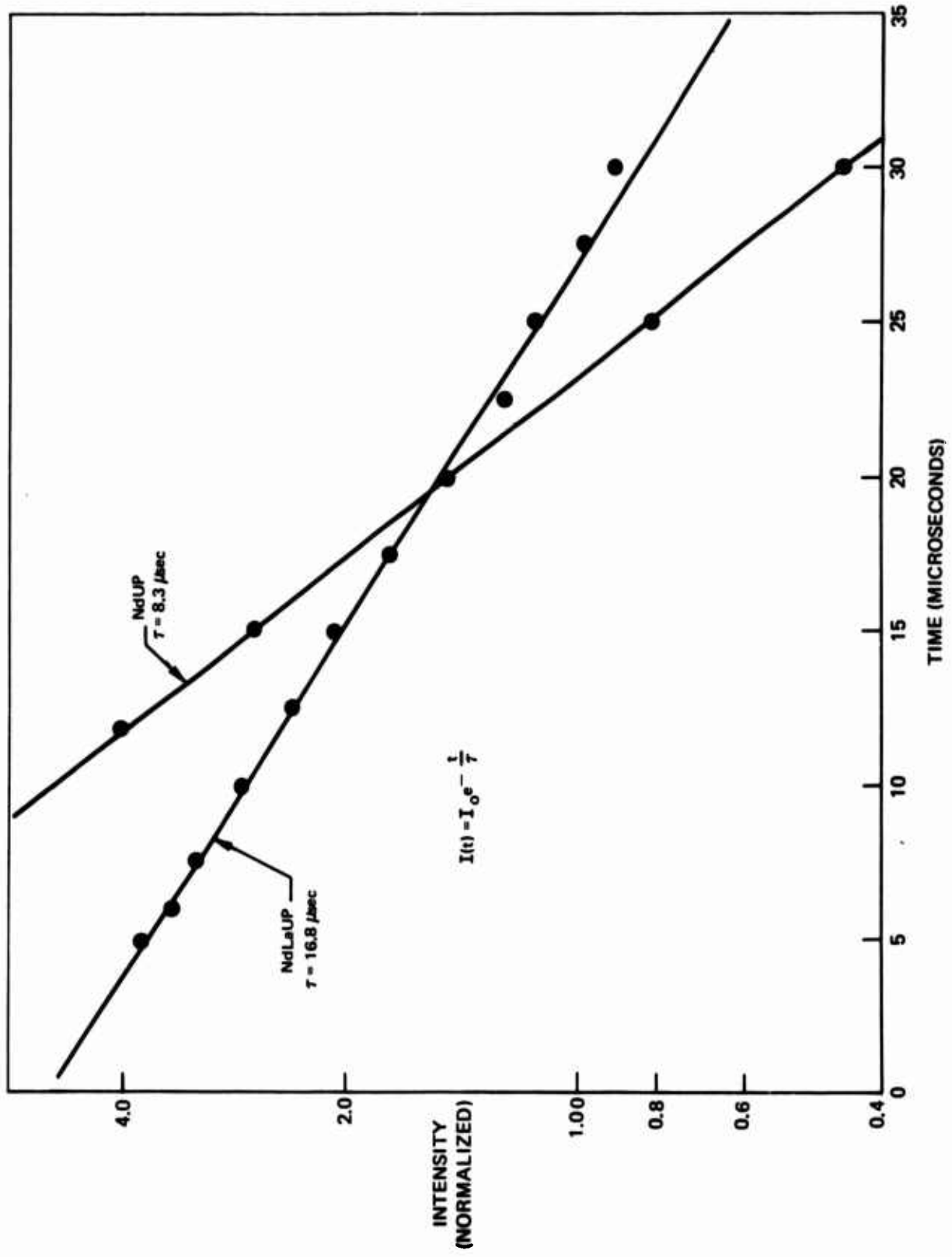

N04–181–2

N82337-12

SCHEMATIC OF WAVEGUIDE ASSEMBLY USED TO DETERMINE OUTPUT EFFICIENCY AND MAXIMUM FILM LOSS

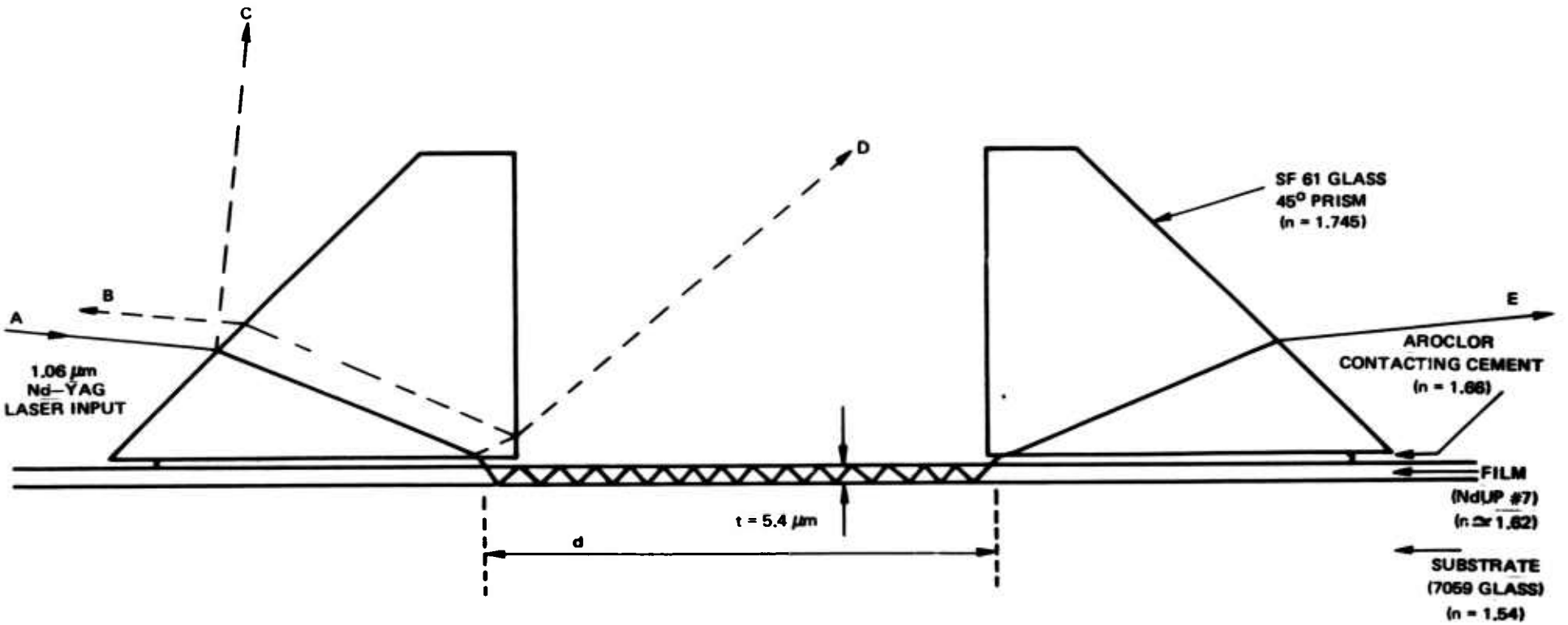

INTENSITY MEASUREMENTS AT 1.06 μm					UNMEASURED LIGHT INTENSITY A–(B + C + D + E)	d(cm)	OUTPUT EFFICIENCY $\frac{100(E)}{A}$	MAX FILM LOSS (dB/cm)
A	B	C	D	E				
850	40	64	490	72	184	2.1	8.5%	2.6
800	30	62	350	110	248	4.1	13.7%	1.25

21

N04-198-1

FIG. 2-8

FIG. 2–9

SCHEMATIC OF THIN FILM LASER CAVITY

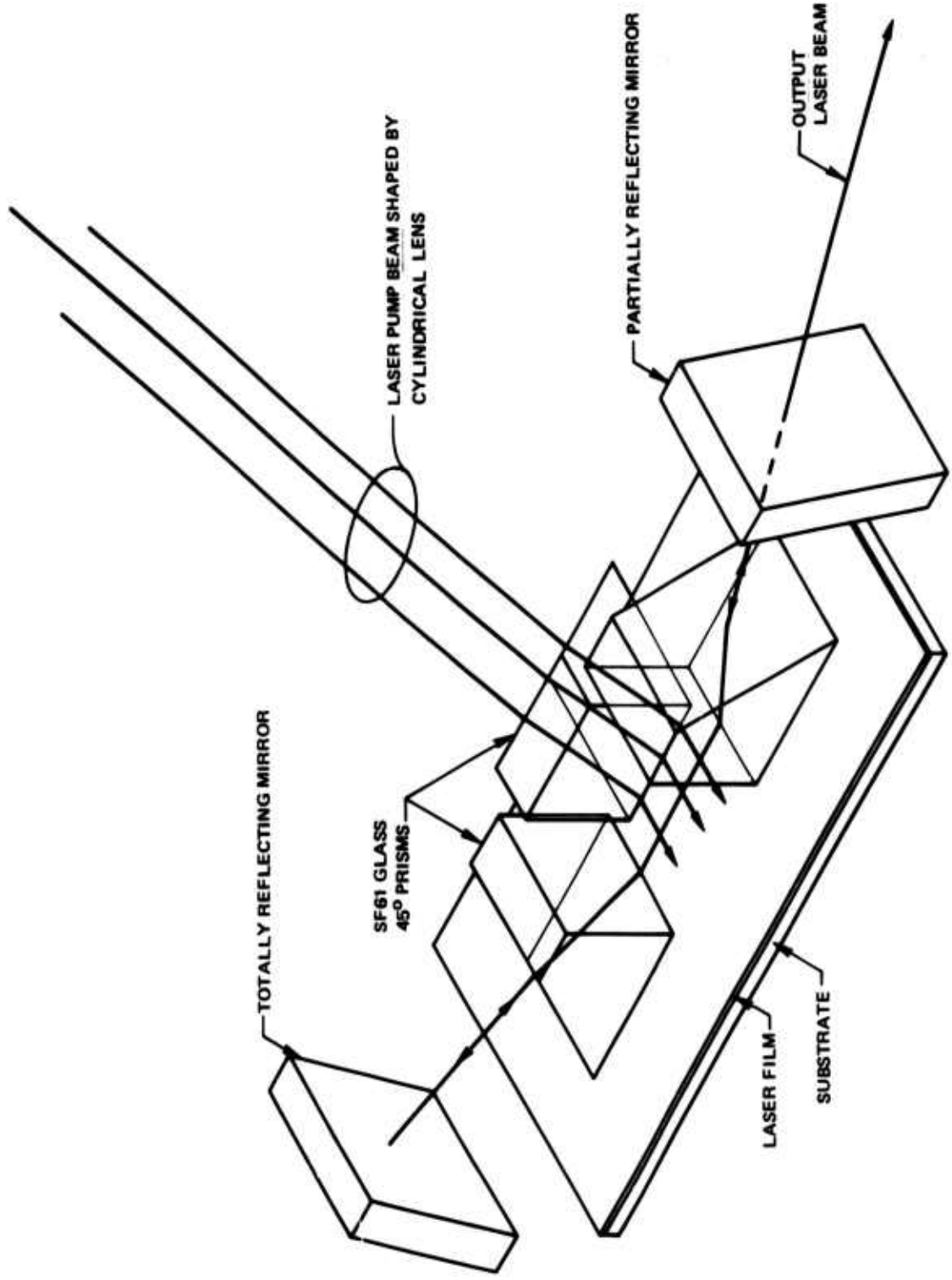

N03–169–1

FIG. 2–10

THIN FILM LASER CAVITY

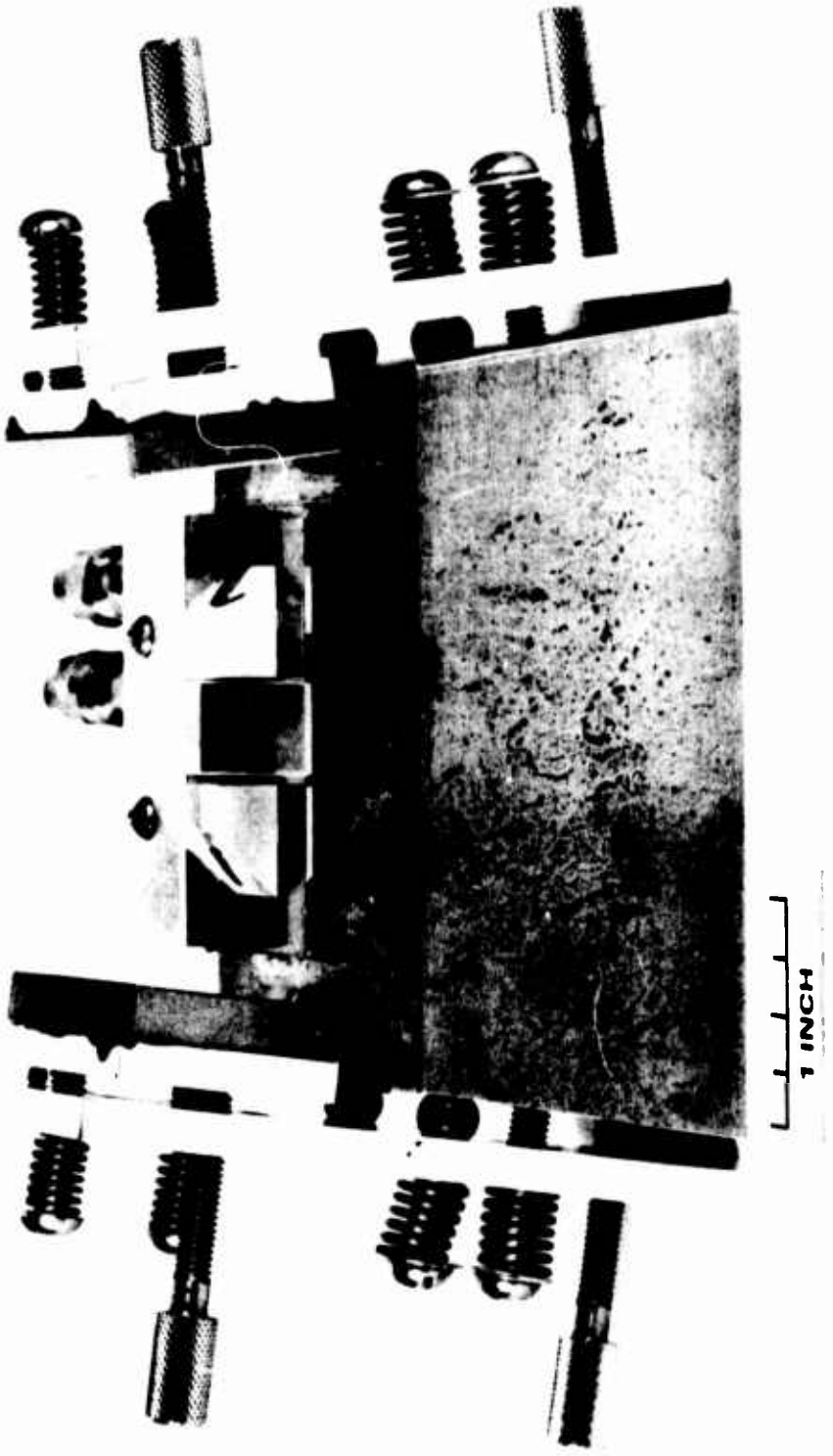

N03–121–1

3.0 GROWTH OF EPITAXIAL GALLIUM ARSENIDE FILMS

As stated in the last report, growth of indium arsenide via sputtering was undertaken in order to optimize the process parameters with respect to the measured electrical properties and then apply these results to the growth of gallium arsenide. Indium antimonide was chosen since it can readily be deposited in thin film form having near bulk-like electrical properties and has the highest reported Hall carrier mobility of all the III-V compounds. Further work into indium antimonide growth during this period led to inconsistent results with regard to the dependence of film integrity (polycrystalline versus single crystal) and electrical properties on growth conditions. These problems were due to the inability to reproducibly control the antimony vapor pressure during sputtering. Two methods were used to establish an antimony pressure in the chamber: (1) evaporate antimony from a heated crucible and (2) sputter elemental antimony off the indium antimonide target. In either case, the 250°C sputtering chamber acts as a "cold" trap for antimony vapor at antimony pressures required for plasma formation. As a result of this, measurement and control of the antimony vapor pressure with an ion gauge (as is possible for arsenic) is impossible. For these reasons, work on sputtered indium antimonide ceased.

Rather than proceeding into rf sputtering of indium arsenide, as suggested in the last report if antimony vapor control proved to be a problem (indium antimonide can be evaporated in thin film form having reasonably high carrier mobility), work again commenced on growing gallium arsenide in order to produce thick layers (> 10 μm) suitable for waveguide evaluation. Typical electrical properties of the sputtered GaAs include high resistivity ($\rho > 10^4 - 10^5$ ohm-cm) and low carrier mobility ($\mu_H < \sim 1$ cm^2/V-sec) and may be useful as a modulator at 1.06 μm. Several layers were grown and tested for waveguide attenuation. Input and output gratings ($d \sim 0.7$ μm) for coupling the 1.06 μm light were fabricated using the interference of two beams split off from a one-watt argon-ion laser onto films which had previously been coated with photoresist (Shipley Type PZ-130). Gratings were also fabricated on amorphous tantalum pentoxide films on 7059 glass and were demonstrated to couple properly using a He-Ne laser. However, the presence of 1.06 μm light guiding in the sputtered layers was not observed. Large attenuation in the film was, therefore, indicated. In an effort to resolve the reason behind the large attenuation, one layer was electron microprobed, and significant quantities of indium and antomony were shown to be present in the gallium arsenide layer. The analysis gave 0.30 and 0.84 atom percents for indium and antimony respectively. This presence of indium and antimony is known to shift the funamental absorption edge to lower energies compared to gallium arsenide. This will result in a larger absorption at 1.06 microns compared to gallium arsenide. Despite the thorough cleaning of several critical parts of the sputtering chamber, measurable concentrations of these contaminants were not expected and necessitated complete dismantling and cleaning (including chemical etching in acid solution) of the sputtering chamber. In the lengthy

process, all the electrical feedthroughs had to be replaced, and the cathode assembly was redesigned to accommodate a new feedthrough. Growth of thick gallium arsenide layers is now in progress.

4.0 EPITAXY OF GALLIUM NITRIDE BY REACTIVE SPUTTERING

Single crystal films of gallium nitride have been prepared by reactive sputtering of gallium in an ammonia ambient. To our knowledge this works constitutes the first successful effort to grow single crystal films of gallium nitride by this technique. Epitaxy has been achieved on (111) oriented substrates of magnesium aluminum spinel and (0001) and (1$\bar{1}$02) oriented sapphire substrates.

Gallium nitride crystallizes in the hexagonal wurtzite structure with unit-cell dimensions a_o = 3.180 Å and c_o = 5,166 Å. It is isomorphous in structure to aluminum nitride and is piezoelectric. Gallium nitride has a direct bandgap of 3.5eV(Ref. 9) and, potentially, junction light emmitting diodes in the blue can be fabricated from it. A disadvantage to material prepared by chemical vapor deposition is that it yields n-type material with a carrier concentration of $\sim 10^{19}/cm^3$, (Ref. 9). Semi-insulating films of gallium nitride can be produced by compensation with zinc during growth. The motivation for growth of gallium nitride by reactive sputtering is to determine if a different method of preparation would result in films with a considerably lower election concentration. If successful, this would provide the basis for preparation of p-type material required for the fabrication of junction light emitting diodes in the blue or a solid state laser in the ultraviolet.

4.1 Epitaxial Thin Film Deposition

The preparation of the sapphire and spinel substrates prior to deposition was the same as that described in a previous report (Ref. 10). A molybenum cathode was fabricated to contain the gallium metal since its melting point is only 30°C. The initial sputtering configuration employed had the gallium source at the bottom of the chamber and the substrate heater assembly suspended above. A number of difficulties were encountered with this arrangement. Flaking of material from the substrate heater contaminated the gallium. The clamping arrangement used to hold the sample in contact with the substrate heater was found to influence film quality in a deleterious fashion. It was required to revise the system to conform to the conventional sputtering geometry with the cathode surpended above the substrate heater. Alcohol and dry ice was used as a coolant to maintain the gallium in solid form even though substrate heater temperatures ranged as high as 1100°C in the course of the experiments. This arrangement proved to be superior although several accidental dumpings of gallium have occurred as a result of cooling system failures.

Single crystal films were grown on (0001) and (1$\bar{1}$02) oriented sapphire substrates. Reflection electron diffraction data of gallium nitride films grown on sapphire are shown in Figures 4-1 and 4-2 for these orientations. The epitaxial relationships for gallium nitride films on sapphire are indtical as that

obtained for aluminum nitride, (0001) planes grow paralled to the surface on (0001) sapphire and (1120) planes paralled to the surface on (1102) sapphires. Epitaxial films were also grown on (111) oriented magnesium aluminum spinel. For this case (0001) planes of gallium nitride grew parallel to the (111) planes of the spinel. Epitaxy was achieved at a substrate temperature as low as 850° but the results obtained were erratic. To date, the deposition parameters established as yielding the best results are:

Reactive Ambient	-	20 mtorr NH_3
Substrate Temperature	-	900°C
Power Density	-	0.8W/cm.^{2}
Deposition Rate	-	40 Å/min

A deposition rates as high as 80 Å/min could be achieved on (0001) oriented films and still maintain single crystal growth. A deposition rate in excess of 40 Å/min on (1102) sapphire substrates would result in polycrystalline deposits. A similar behavior was also observed for aluminum nitride. The major efforts on gallium nitride have been directed primarily toward sputtering system refinements and the determination of deposition parameters for epitaxy. Therefore, evaluation of the material has been limited primarily to film structure. Preliminary measurements on the electrical characteristics of the material indicate that the films grown are high resistivity.

4.2 Future Work

The piezoelectric properties of the film will be evaluated by fabrication of surface acoustic delay lines. Optical waveguiding properties of the films will be assessed. Modification of the electrical properties of the gallium nitride films by doping will be explored.

FIG. 4–1

RED OF GaN ON (0001) Al_2O_3

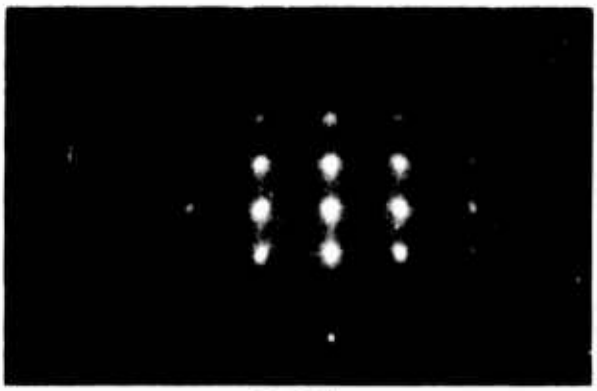

[1120]

[1010]

RED OF GaN ON (IT02) Al_2O_3

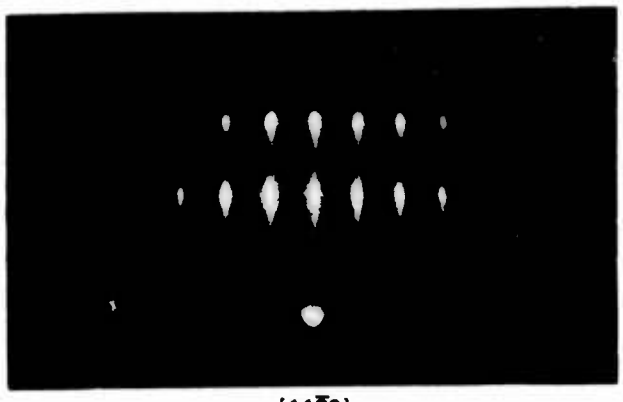

[$11\bar{2}0$]

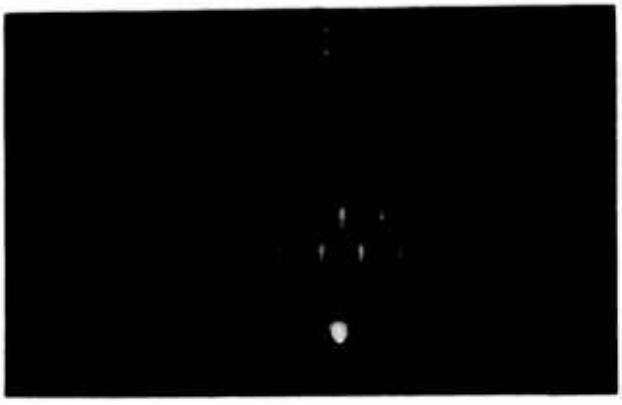

[0001]

5.0 TUNGSTEN TRIOXIDE

Epitaxial growth of tungsten trioxide has been obtained on (110) spinel and (1102) sapphire substrates. The tungsten trioxide grows with (010) planes parallel to the film surface. The films are twinned as a result of domain formation. This is illustrated by the reflection electron diffraction patterns shown in Figure 5-1. The twinning results from the phase changes the crystal passes through upon cooling. Film deposition generally takes place at temperatures in excess of 800°C. Tungsten trioxide upon cooling passes from the tetragonal phase to orthorhombic at ∿ 710°C and from orthorhrombic to monoclinic at 330°C. In bulk single crystals the domains can be removed by a properly applied stress. In the thin film heteroeptiaxial structures the domain walls are pinned and no way has been found to create a single domain film. The twinning gives rise to excessive scattering loss in optical waveguide structures which precludes the use of this material for intergrated optics.

Growth was achieved at substrate temperatures ranging between 800-850°C, an oxygen pressure of 20 mTorr and an rf power density of $4 W/cm^2$. Target to substrate separation was 2.5 cm. The films which were grown were insulating.

REFLECTION ELECTRON DIFFRACTION PATTERNS FOR WO_3 ON $(1\bar{1}02)$ SAPPHIRE

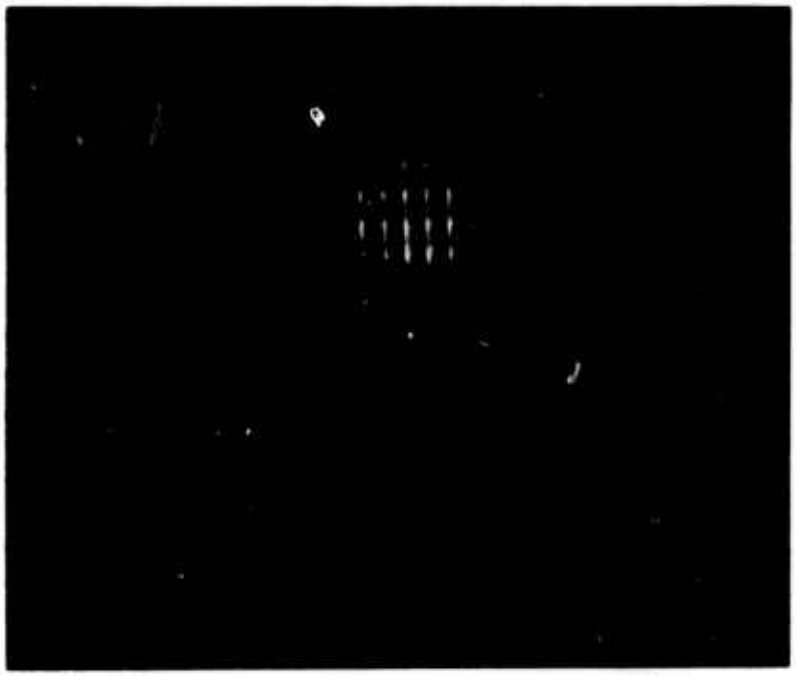

ELECTRON BEAM DIRECTED ALONG [101]

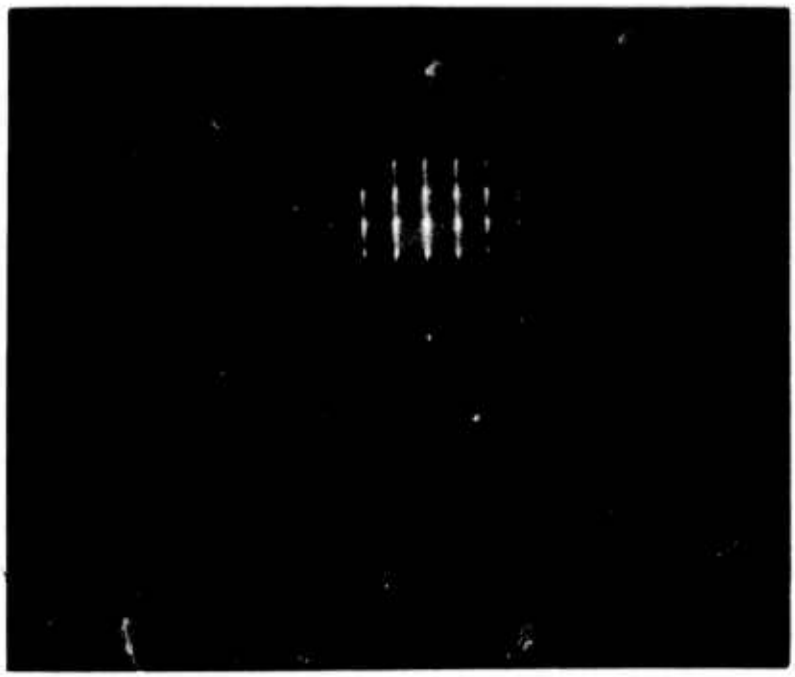

ELECTRON BEAM DIRECTED ALONG [100]

6.0 OPTIMIZATION OF ZINC OXIDE DEPOSITION PARAMETERS

Efforts continued to optimize the sputtering parameters for the growth of low optical loss single crystal ZnO. The parameters investigated were magnetic field strength and contour at the target surface, substrate heater temperature, rf input power to the target, and sputtering gas pressure.

6.1 Magnetic Field Experiments

Previous work in sputtering polycrystalline films of ZnO indicated that films grown near the center of the substrate holder were very grainy while films grown near the outer edge of the substrate holder were much less grainy for a given sputtering power level. It was also observed that the degree of graininess increased with increasing power input to the target. Brodie, Lamont and Myers (Ref. 11) have shown that reducing substrate bombardment by the secondary electrons resulted not only in reducing heat dissipated at the substrate but also in improving the texture of the sputtered films. Kay (Ref. 12) has shown that a quadrupole magnetic field superimposed between the target and substrate can effect the temperature distribution at the substrate. His results showed that while the deposition rate and temperature were subtantially increased at the center of the substrate holder, the temperature at the outer edge of the substrate holder was depressed. For this reason the quadrupole field was investigated.

The major internal components of the sputtering system used for these experiments are illustrated schematically in Figure 6-1. A special feature of the sputtering system is the variety of magnetic fields which can be produced in the region of the substrate and cathode. The fields are produced by a pair of solenoids each about 1.27 cm long, 17.8 cm inside diameter and 25 cm outside diameter. Each coil has 12 turns of water-cooled copper conductor. Electrical currents of over 450 amps d.c. can be maintained indefinitely without raising the coil temperature beyond 50°C. The coils are coaxial with the cathode and substrate holder. Figure 6-1 illustrates the relative position of these components. Spacing between the coils and position of the coil pair midplane are variable over a range of about 15 cm. The target-to-substrate distance was maintained at 3.25 cm for these experiments. The coils can be connected so that their fields either add or oppose. In this way, the magnetic field can be changed from a predominantly longitudinal one to a quadrupole one.

Temperature measurements were made at six locations along a radius of the substrate holder for various magnetic field strengths and configurations. The temperature sensors were made from a 1.27 cm diameter by 0.55 cm high stainless steel rod with a chromel-alumel thermocouple spot welded in a 0.30 cm deep groove on the underside of the steel slug. The sensors were held in place simply by

their own weight. Thermal contact with a constant temperature substrate holder was intentionally poor to simulate the case where substrates are normally held to the holder by their own weight. The substrate holder temperature is controllable and was kept at a constant 10°C. Sensor temperatures were recorded before start up of each run so that the raise in temperature could be determined. Sensor temperatures were normally between 10 and 20°C at start-up.

The sputtering target was a 15.25 cm diameter hot pressed ZnO disc. The rf power input to the target for this series of tests was 5.5 watts/cm^2. Essentially equilibrium temperature of the sensors was arrived at after about 10 minutes of operation (Figure 6-2). Temperature profiles were taken after 11.5 minutes of operation and for many of the same runs after only 1.5 minutes of operation. In general, the shape of the temperature profile for the shorter runs was similar to that for the longer runs. However, temperatures were much higher for the longer runs.

The sputtering gas was an 80 - 20 percent mixture of argon and oxygen at 10 mtorr.

A variety of coil pair positions and separation distances as well as field strength were investigated to determine their effect on the substrate temperature profile. Curve 1 of Figure 6-3 shows the temperature profile as well as the film thickness profile obtained for the configuration which produced the lowest substrate temperature at the outer radius. However, the deposition profile for the outer 4.5 cm shown that the deposition rate can fall off by nearly a factor of two in the outer 3 cm. This is not too surprising when the deposition profile for the case with no magnetic field is considered (curve II, Figure 6-3). For the latter case, nearly the same percentage of rate loss is experienced. For the zero magnetic field, however, the overall rate is less and the temperature is greater at the outer edge than that for the applied quadrupole field. Curve III, Figure 6-3, illustrates yet another example where a further increase in rate is accompanied by a much greater heating effect. This condition was produced by moving the quadrupole field midplane to within 0.2 cm of the target. An increase in deposition rate as the midplane of the quadrupole field is brought in the vicinity of the target cathode dark space, is predicted by Kay.

Duplicate experiments were run with the magnetic fields of the coil pair arranged to add. This produced a predominantly longitudinal field with the axis of the field coincident with the central axis of the target and substrate. A coil pair arrangement was found where the temperature at the center of the substrate holder was depressed while the temperature at the outer edge was increased.

Figure 6-4 shows profiles of the temperature and deposition rate for the condition with maximum magnet current available and the configuration which yielded the lowest substrate central temperature. For comparison, similar data

is presented for the zero magnetic field case. Note that these two runs were made at an input rf power to the target of 2.75 watts/cm^2, half of that used for the other runs in these experiments. The deposition rate at the center has not been increased by the use of the longitudinal field over the zero magnetic field case; however, the rise in temperature of the substrate due to the energetic secondary electron bombardment is substantially reduced. On the other hand, the deposition profile with the longitudinal magnetic field has been considerably flattened over that of the quadrupole field case. the profile is flat to within $\pm$ 10% over the entire 15 cm diameter and to within about 2.5% over the central 5 cm.

For the conditions corresponding to curve 1 of Figure 6-4, several depositions of ZnO were made on polished single crystal (1$\bar{1}$02) oriented sapphire substrates. The substrates were placed at the center of the substrate holder. Figure 6-5 is a comparison photomicrograph of the ZnO coated substrates for two values of the longitudinal magnetic field. The higher magnetic field, which is the condition of curve I, Figure 6-4, clearly shows a much improved film texture.

6.2 Substrate Heater Temperature Experiments

While the results of the magnetic field experiments indicated that substrate heating by secondary electron bombardment was undesirable in obtaining smooth films, the need for substrate heating for the production of single crystal films was still found to be necessary.

Substrates were heating by placing them directly on to a tantalum heater strip. ZnO films were grown at temperatures ranging from 825°C down to 225°C. The higher temperatures produced the best quality single crystal as evidenced by the sharp reflection electron diffraction spot patterns and the accompanying Kukuchi line patterns. However, the films had a tendency to grow crystal projections on the surface. At a substrate heater temperature of 825°C, the projections were estimated to be about 1.5μ in height and 3μ in diameter. The result of the presence of these projections was not only to make it very difficult to couple light into the films, since the prism couplers require close contact with the film but also to present additional opportunities for the light to be scattered out of the film. These films exhibited no light guiding.

At a heater temperature about 600°C, the faceting of the films on (1$\bar{1}$02) sapphire had disappeared. However, the films grown on the (0001) sapphire were no longer single but had deteriorated to oriented polycrystalline and polycrystalline. Below 500°C the (1$\bar{1}$02) films showed an increased tendency to form twinned crystals. Twinned crystals were grown at heater temperature as low as 225°C on (1$\bar{1}$02) sapphire. Many of these twinned films guided .6328μ light albeit with losses of about 20 db/cm.

6.3 Target Power Input Experiments

The experiments with substrate heater temperature described in the previous section were conducted with a power input to the target of 0.69 watts/cm^2. Increasing the power to 2.2 watts/cm^2 at a substrate heater temperature of 475°C produced oriented polycrystalline films on both the (0001) and (1$\bar{1}$02) sapphire. However, reducing the power input to 0.22 watts/cm^2 at the same heater temperature resulted in producing single crystal films on both the (0001) and (1$\bar{1}$02) substrates. The ZnO film grown on the (1$\bar{1}$02) resulted in the best .6328μ light guide produced on this substrate orientation by us to date.

The single crystal film grown on the (0001) substrate, however, showed the presence of hexagonal shaped projections rising up from the surface.

Since 0.22 watts/cm^2 power input to the target represents only 40 watts of rf power into the system, the limits of stability of both the rf power supply as well as the plasma in the sputtering chamber were being approached. For these reasons per the reduction in power were not attempted.

6.4 Gas Pressure Experiments

All of the previous studies were made at a total sputtering gas pressure of 10 mTorr. Increasing the total gas pressure to 30 mTorr while maintaining the ratio of 80% Ar and 20% O_2 resulted in reducing the amount of faceting on the (0001) substrate. The other system parameters were maintained at those conditions which had been shown to optimize the film growth under the conditions studied. That is, the magnets were in the longitudinal configuration with a current of 400 amps through the coils; the heater temperature was set at 475°C; the rf power input density was 0.22 watts/cm^2.

The sputtering gas pressure was further increased to a total pressure of 50 mTorr. This resulted in virtual elimination of the faceting and produced the conditions for the best guiding of .6328μ light in ZnO films grown of (0001) sapphire substrates. Figure 6-6 is the attenuation data obtained with this film and indicates a loss of 5.3db/cm.

FIG. 6–1

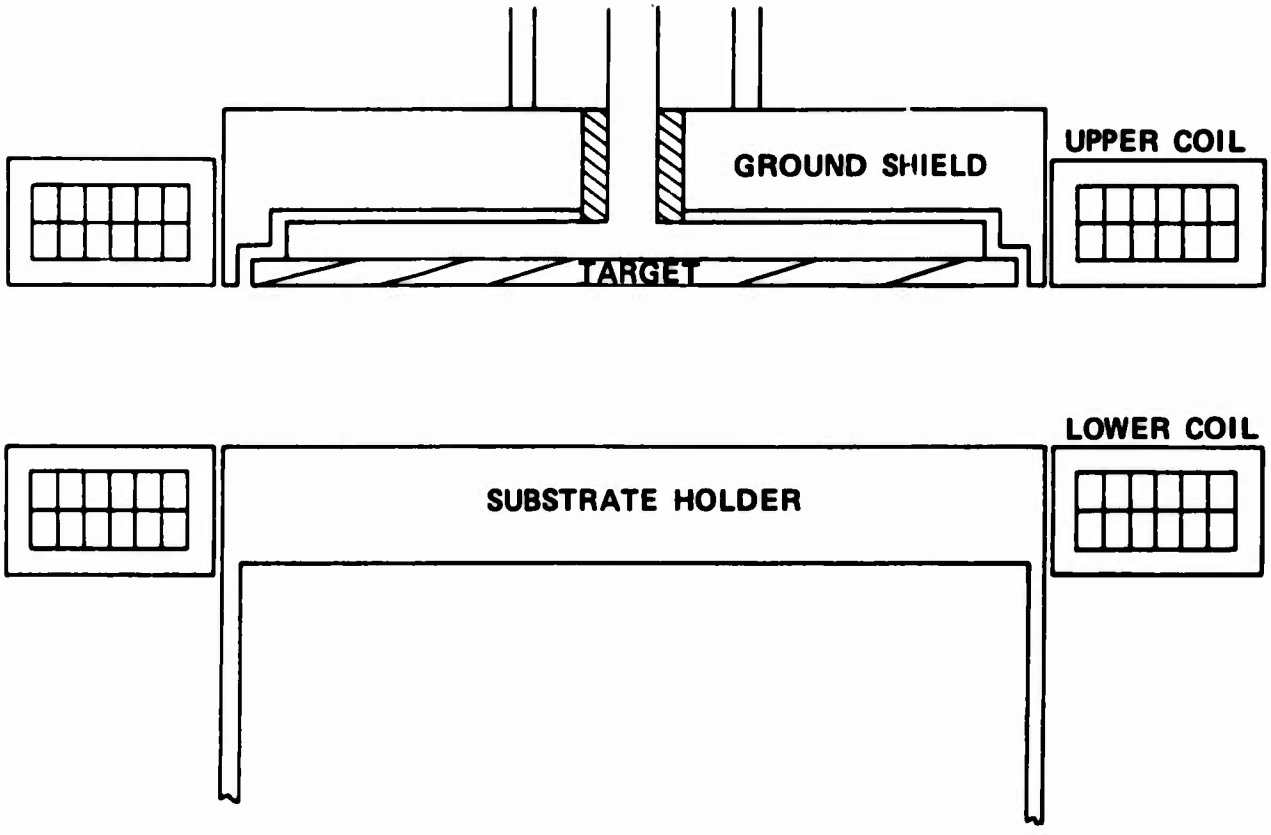

N04–106–2

FIG. 6-2

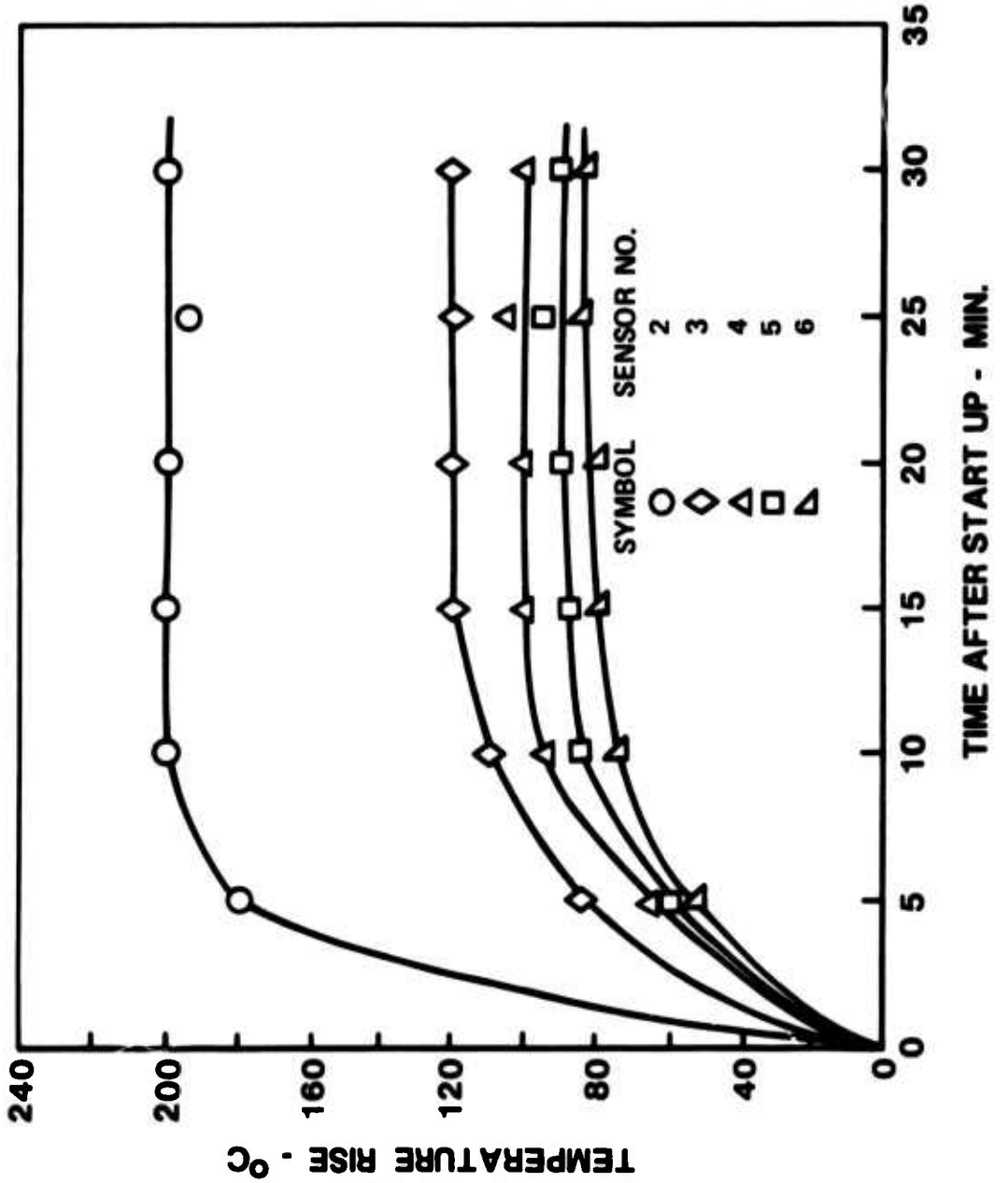
TEMPERATURE RISE - °C
240
200
160
120
80
40
0
0
5
10
15
20
25
30
35
TIME AFTER START UP - MIN.
SYMBOL SENSOR NO.
2
3
4
5
6
N04-143-2

FIG. 6-3

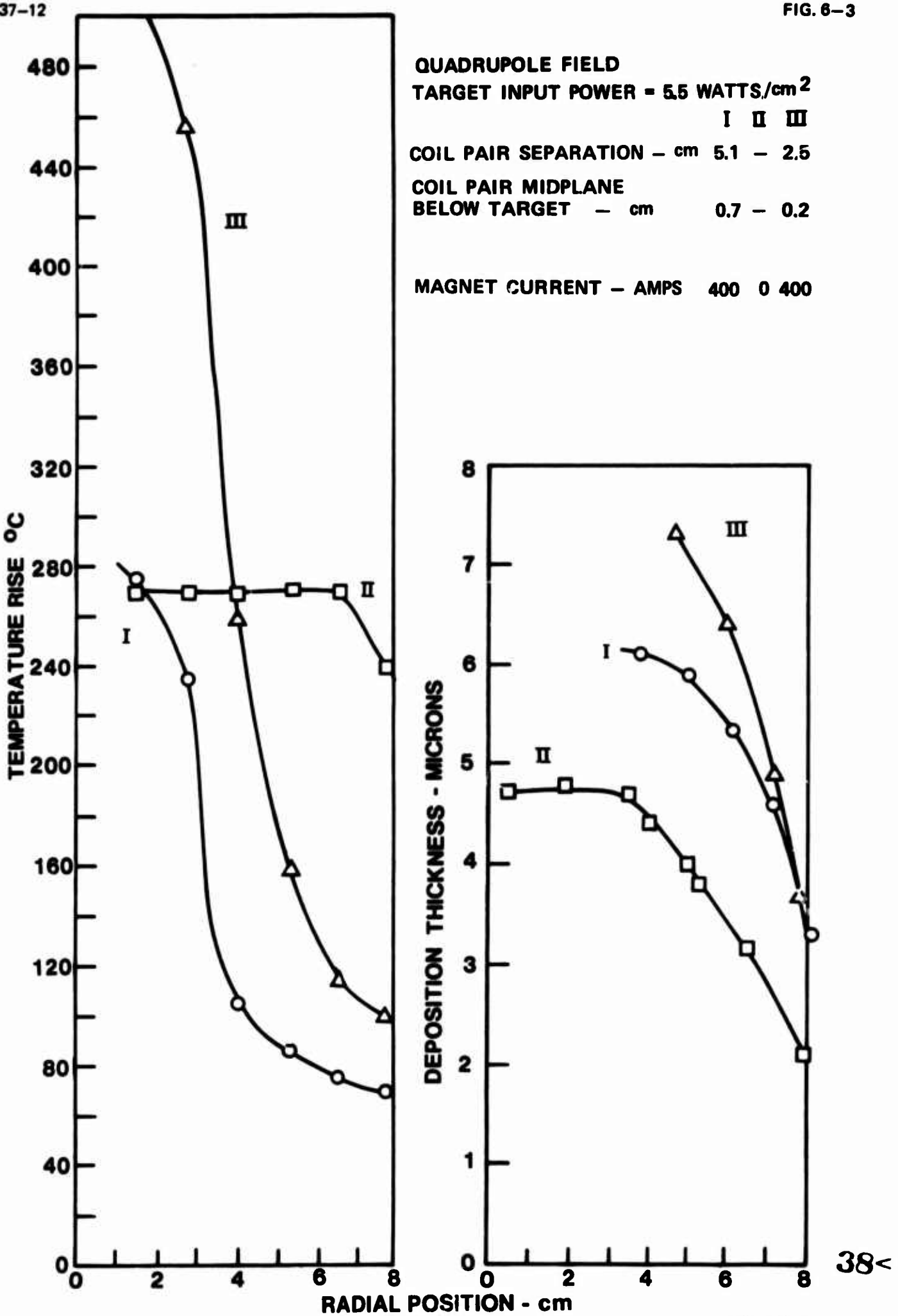

N04-106-5

FIG. 6-4

LONGITUDINAL FIELD
TARGET INPUT POWER – 2.75 WATTS/cm^2

	I	II
COIL PAIR SEPARATION – cm	2.5	–
COIL PAIR MIDPLANE BELOW TARGET – cm	1.8	–
MAGNET CURRENT – AMPS	400	0

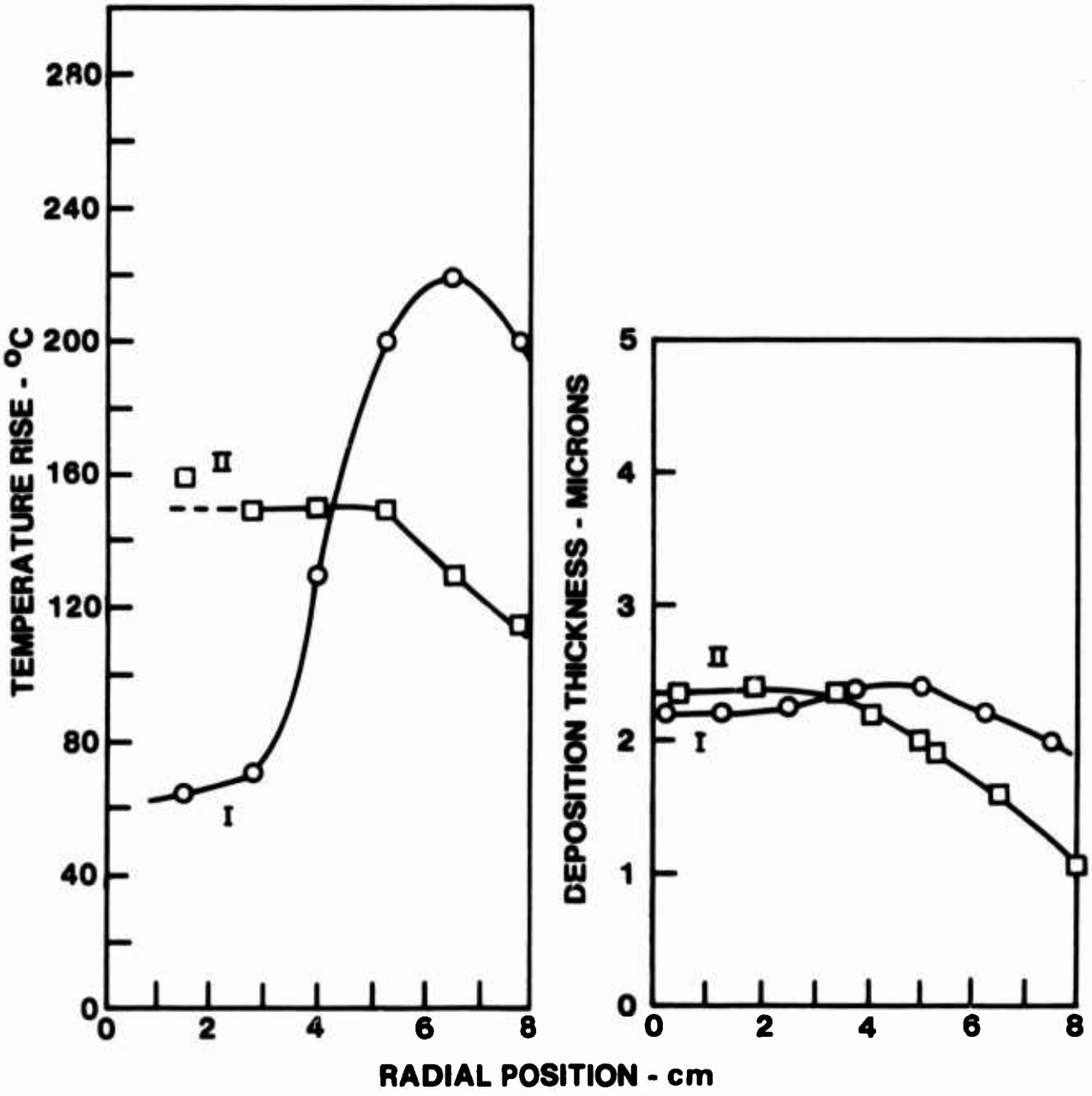

N04-106-1

FIG. 6-5

N04-143-1

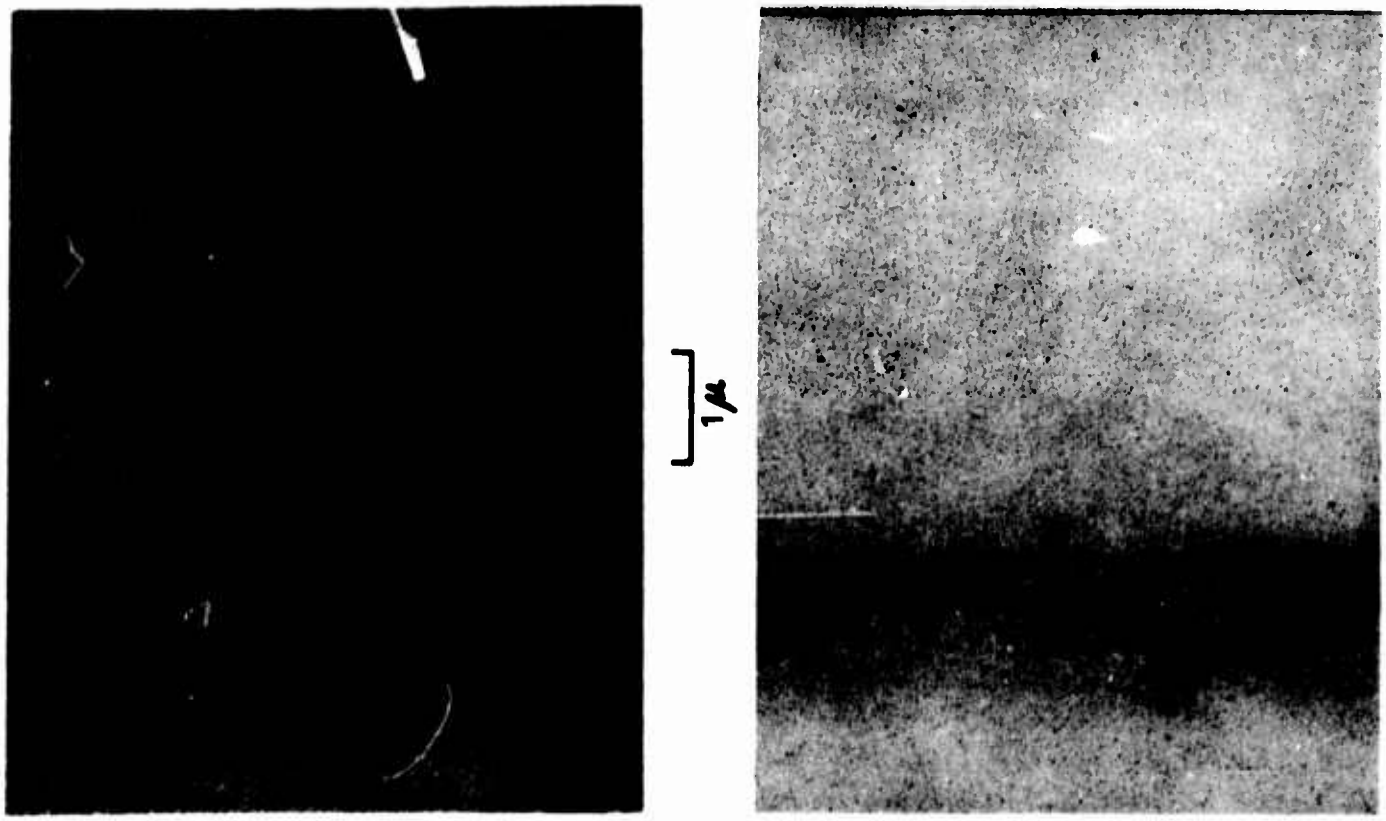

FIG. 6–6

N04–143–7

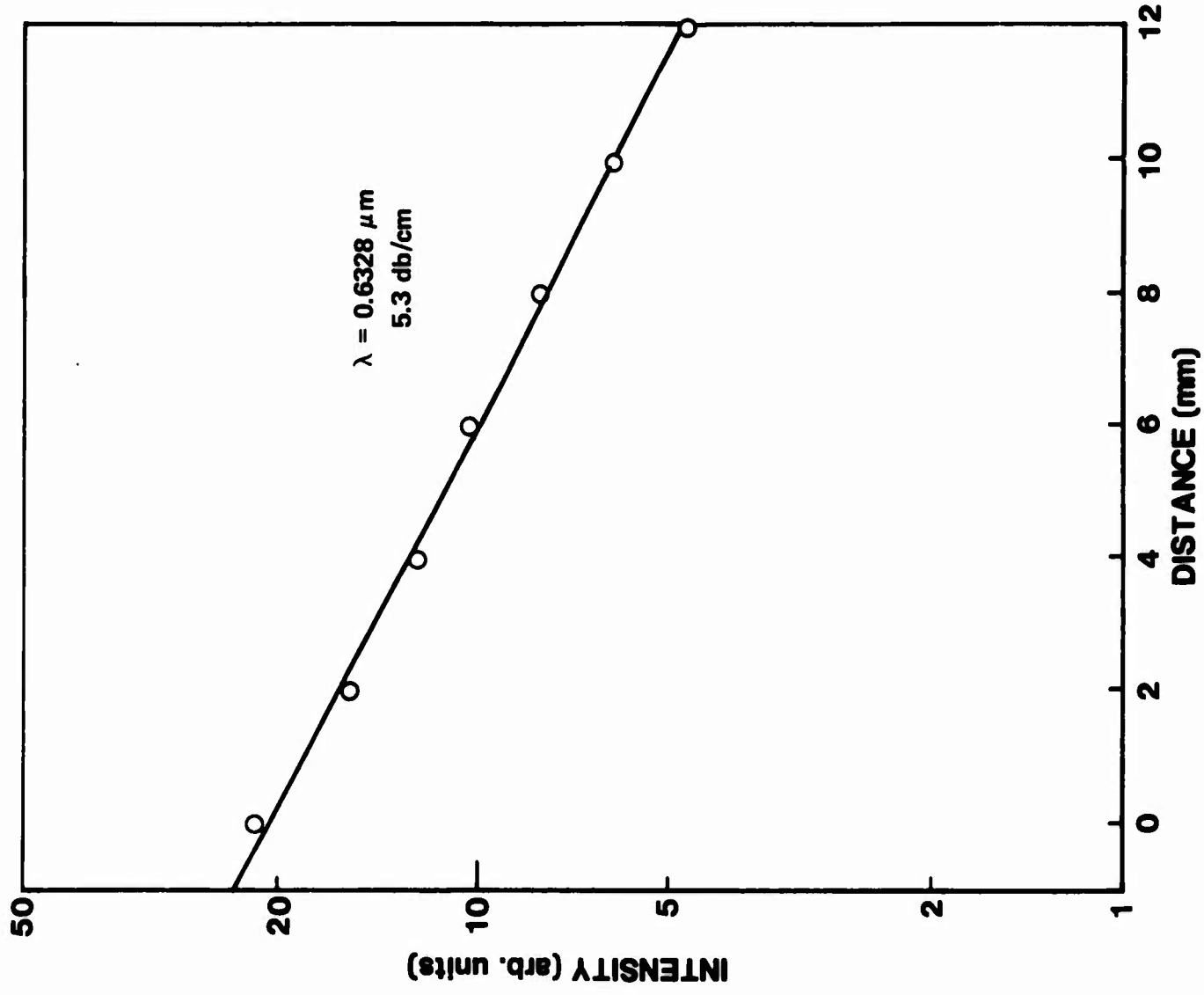

7.0 REFERENCES

1. H. P. Weber, B. C. Tofield, and T. C. Damen, Topical Meeting on Integrated Optics, Paper MB8-1, New Orleans, 1974.

2. H. G. Danielmeyer and H. P. Weber, J of Quant. Electr. QE-8, 805-8 (1972).

3. H. G. Danielmeyer, J. P. Jeser, E. Schonherr, and W. Stetter, J. of Crystal Growth (1974), to be published.

4. R. D. Maurer, Proceedings of the Symposium on Optical Lasers, (New York, Polytechnic Press), Vol. XIII, pg. 435 (1963).

5. H. P. Weber, T. C. Damen, H. G. Danielmeyer and B. C. Tofield, Appl. Phys. Lett. 22, 534 (1973).

6. W. W. Kruhler, J. P. Jeser, H. G. Danielmeyer, Appl. Phys. 2, 329 (1973).

7. H. G. Danielmeyer, G. Huber, W. W. Kruhler and J. P. Jeser, Appl. Phys. 2, 335 (1973).

8. T. C. Damen, H. P. Weber and B. C. Tofield, Appl. Phys. Lett. 23, 519 (1973).

9. J. I. Pankow, H. P. Maruska and J. E. Berkyheiser, Appl. Phys. Lett. 17, 197 (1970).

10. Sputtered Thin Film Research, Second Semi-Annual Technical Report, ONR Contract No. N00014-72-C-0415, May, 1973.

11. I. Brodie, L. T. Lamont, and D. O. Meyers, J. Vac. Sci. Technol. 6, 124 (1969).

12. E. Kay, J. Appl. Phys. 34, 760 (1963).